

ACCELERATED GRADIENT FLOWS FOR LARGE BENDING DEFORMATIONS OF NONLINEAR PLATES

GUOZHI DONG*, HAILONG GUO†, AND SHUO YANG‡

Abstract. In this paper, we propose and analyze a series of novel algorithms based on projection-free accelerated gradient flows to minimize bending energies for nonlinear plates with non-convex metric constraints. We discuss the stability and constraint consistency in a semi-discrete setting for both bilayer and prestrained plates. Our proposed algorithms demonstrate substantial improvements, in both efficiency and accuracy, over current state-of-the-art methods based on gradient flows.

Key words. Accelerated gradient flows, projection-free, bilayer plates, prestrained plates, energy stability

MSC codes. 65N12, 65K10, 74K20, 35Q90

1. Introduction. Large spontaneous deformations of nonlinear plates have recently attracted significant attention in materials engineering and applied mathematics due to their broad applications in natural phenomena and engineered devices. Examples include the snapping behavior of the venus flytrap [24], the natural growth of soft tissues in plant leaves and blossoms [25], cell encapsulation devices [37] and self-deploying solar sails [28].

1.1. Models. In mathematical models of nonlinear plates, deformations of materials are described by $\mathbf{y} : \Omega \rightarrow \mathbb{R}^3$, where $\Omega \subset \mathbb{R}^2$ represents a bounded Lipschitz domain. Equilibrium deformations are minimizers of bending energies under metric constraints for the deformed surfaces \mathbf{y} . This work is specifically focused on the computational methods for *bilayer plates* and *prestrained plates*.

1.1.1. Bilayer plates. We consider a model of bilayer plates that was developed and analyzed in [35, 36, 8]. In this model, we seek equilibrium deformations by solving the following constrained minimization problem

$$(1.1) \quad \min_{\mathbf{y} \in \mathcal{A}} E_{bi}[\mathbf{y}] := \min_{\mathbf{y} \in \mathcal{A}} \frac{1}{2} \int_{\Omega} |D^2 \mathbf{y}|^2 - \sum_{i,j=1}^2 \int_{\Omega} \partial_{ij} \mathbf{y} \cdot (\partial_1 \mathbf{y} \times \partial_2 \mathbf{y}) Z_{ij},$$

where $Z \in [L^\infty(\Omega)]^{2 \times 2}$ represents the *spontaneous curvature* that reflects the materials characteristics of the bilayer plates. Essentially, the presence of Z drives the plate $\mathbf{y}(\Omega)$ to deform out of plane and achieve non-trivial shapes. We further define the non-convex term of E_{bi} as $E_{bi}^{nc} := - \sum_{i,j=1}^2 \int_{\Omega} \partial_{ij} \mathbf{y} \cdot (\partial_1 \mathbf{y} \times \partial_2 \mathbf{y}) Z_{ij}$, and convex terms as $E_{bi}^c = E_{bi} - E_{bi}^{nc}$.

The *admissible set* \mathcal{A} , which prevents shearing and stretching within the surface $\mathbf{y}(\Omega)$ and imposes possible boundary conditions, are defined as follows:

$$(1.2) \quad \mathcal{A} := \{ \mathbf{y} \in [H^2(\Omega)]^3 : \quad \mathbb{I}[\mathbf{y}] = I_2 \text{ in } \Omega, \quad \mathbf{y} = \boldsymbol{\varphi}, \quad \nabla \mathbf{y} = \Phi \text{ on } \Gamma^D \}.$$

*School of Mathematics and Statistics, HNP-LAMA, Central South University, Changsha 410083, China (guozhi.dong@csu.edu.cn).

†School of Mathematics and Statistics, The University of Melbourne, Parkville, VIC, 3010, Australia (hailong.guo@unimelb.edu.au).

‡Beijing Institute of Mathematical Sciences and Applications, Beijing, 101408, China (shuoyang@bimsa.cn).

Here $I[\mathbf{y}]$ is the first fundamental form of $\mathbf{y}(\Omega)$, i.e.

$$(1.3) \quad I[\mathbf{y}] := \nabla \mathbf{y}^T \nabla \mathbf{y},$$

and I_2 is the 2×2 identity matrix, $\Gamma^D \subset \partial\Omega$ stands for the part of boundary where Dirichlet boundary conditions are imposed. We assume that the boundary data $\boldsymbol{\varphi} \in [H^2(\Omega)]^3$ and $\Phi \in [H^1(\Omega)]^{3 \times 2}$ are given and compatible with the isometry constraint, namely $\Phi = \nabla \boldsymbol{\varphi}$ and $\Phi^T \Phi = I_2$ on Γ_D ; thus \mathcal{A} is non-empty. It is worth noting that both the bending energy $E_{bi}[\mathbf{y}]$ and the constraint $I[\mathbf{y}] = I_2$ are *non-convex* in this model.

In a specific scenario where two layers have identical materials properties, resulting in $Z = \mathbf{0}$, the model simplifies into *single layer plates* [5, 17], which corresponds precisely with the classical nonlinear Kirchhoff plates theory. In this case, the plate no longer exhibits spontaneous deformations and the energy becomes convex. To induce deformation, we introduce an external force field $\mathbf{f} \in [L^2(\Omega)]^3$ to act upon the plates. The equilibrium deformations of single layer plates solve

$$(1.4) \quad \min_{\mathbf{y} \in \mathcal{A}} E_{si}[\mathbf{y}] := \min_{\mathbf{y} \in \mathcal{A}} \frac{1}{2} \int_{\Omega} |D^2 \mathbf{y}|^2 - \int_{\Omega} \mathbf{f} \cdot \mathbf{y}.$$

1.1.2. Prestrained plates. For prestrained plates, we define a target metric $g \in [H^1(\Omega) \cap L^\infty(\Omega)]^{2 \times 2}$, a given symmetric positive definite matrix-valued function, and deformations belong to the following admissible set

$$(1.5) \quad \mathcal{A}_g := \{\mathbf{y} \in [H^2(\Omega)]^3 : I[\mathbf{y}] = g \text{ in } \Omega, \quad \mathbf{y} = \boldsymbol{\varphi}, \nabla \mathbf{y} = \Phi \text{ on } \Gamma^D\}.$$

Moreover, we assume that g admits *isometric immersions*, i.e., there exists $\mathbf{y} \in [H^2(\Omega)]^3$ such that $\nabla \mathbf{y}^T \nabla \mathbf{y} = g$ a.e., and again the boundary data $\boldsymbol{\varphi} \in [H^2(\Omega)]^3$ and $\Phi \in [H^1(\Omega)]^{3 \times 2}$ are compatible with g , namely $\Phi = \nabla \boldsymbol{\varphi}$ and $\Phi^T \Phi = g$ on Γ_D . These assumptions guarantee that the admissible set \mathcal{A}_g is nonempty.

We consider the bending energy model for isotropic prestrained plates that was proposed in [23] and derived rigorously via Γ -convergence in [10]. We refer to [14] for a formal derivation. The equilibrium deformation is a solution of

$$(1.6) \quad \min_{\mathbf{y} \in \mathcal{A}_g} E_{pre}[\mathbf{y}] := \min_{\mathbf{y} \in \mathcal{A}_g} \frac{\mu}{12} \int_{\Omega} \left| g^{-\frac{1}{2}} D^2 \mathbf{y} g^{-\frac{1}{2}} \right|^2 + \frac{\lambda}{2\mu + \lambda} \text{tr} \left(g^{-\frac{1}{2}} D^2 \mathbf{y} g^{-\frac{1}{2}} \right)^2,$$

where λ and μ are Lamé parameters of the material. For the sake of concise presentation, although $D^2 \mathbf{y}$ is $3 \times 2 \times 2$ -tensor valued, we here define $g^{-\frac{1}{2}} D^2 \mathbf{y} g^{-\frac{1}{2}} := (g^{-\frac{1}{2}} D^2 y_m g^{-\frac{1}{2}})_{m=1}^3$ with $\mathbf{y} := (y_m)_{m=1}^3$, and this is also a $3 \times 2 \times 2$ -tensor. Note that in (1.6) the energy E_{pre} is quadratic (thus convex), while the constraint is still *non-convex*.

In the special case $g = I_2$ (i.e., when \mathbf{y} is an isometry), adding an external force $\mathbf{f} \in [L^2(\Omega)]^3$, the model (1.6) also reduces to the nonlinear Kirchhoff plate model with isometry constraint, i.e. the model for single layer plates, as in (1.4), up to a multiplicative constant depending on λ and μ .

1.2. Previous numerical methods for nonlinear plates. Numerically solving the constrained problems (1.1) and (1.6) presents a nontrivial challenge, primarily because of their inherent non-convexity. Various numerical methods have been devised to tackle these problems. These methods entail constructing proper discrete counterparts of (1.1) and (1.6) and designing effective iterative schemes for solving these non-convex constrained minimization problems.

From the aspect of optimization, most existing works for nonlinear plates resort to gradient flow type iterative schemes. For prestrained and single layer plates, i.e. when the energy is quadratic, the semi-implicit backward Euler scheme is considered in [5, 17, 15], whose semi-discrete formulation formally reads

$$(1.7) \quad \tau^{-1}(\mathbf{y}^{n+1} - \mathbf{y}^n) + \delta E[\mathbf{y}^{n+1}] = \mathbf{0},$$

where \mathbf{y}^n is a given previous step of iteration, $\tau > 0$ is a time step parameter and δE represents the first variation of energy functional $E = E_{pre}$ or E_{si} . Unconditional energy stability is proved in these works. Moreover, the algorithm in [27] employs the combination of an adaptive time-stepping gradient flow and a Newton's method for single layer plates model.

For bilayer plates, where the energy is non-convex, the gradient flow in [8] treats the energy implicitly as in (1.7), while embedding a fixed point sub-iteration to solve the ensuing nonlinear problem. In contrast, [9, 18] make the troubling term explicit and keep the convex part implicit in gradient flows, namely

$$(1.8) \quad \tau^{-1}(\mathbf{y}^{n+1} - \mathbf{y}^n) + \delta E_{bi}^c[\mathbf{y}^{n+1}] + \delta E_{bi}^{nc}[\mathbf{y}^n] = \mathbf{0},$$

and show a conditionally energy decreasing property with a mild time-step constraint.

Regarding the treatment of non-convex metric constraint $\mathbf{I}[\mathbf{y}] = g$ in the optimization process, all aforementioned gradient-flow based FEM works linearize the constraint at each iteration \mathbf{y}^n by requiring increments $\delta \mathbf{y}^{n+1} := \mathbf{y}^{n+1} - \mathbf{y}^n$ in (1.7) and (1.8) belong to a tangent space of the constraint:

$$(1.9) \quad \{\mathbf{v} : L[\mathbf{y}^n; \mathbf{v}] := \nabla \mathbf{v}^T \nabla \mathbf{y}^n + (\nabla \mathbf{y}^n)^T \nabla \mathbf{v} = \mathbf{0}\}.$$

This method naturally compares to the projection-free gradient flows in the study of harmonic maps and liquid crystals; see [6, 32]. Although the constraint is linearized and thus violated in iterations, its violation is proved to be controlled linearly in time step τ .

From the aspects of spatial discretization, several finite element methods (FEM) were designed for (1.1), (1.4) and (1.6) (recall that (1.4) is a special case of (1.1) and (1.6)) and analyzed in the framework of Γ -convergence. In [5, 17, 27], Kirchhoff FEM, interior penalty discontinuous Galerkin (IPDG) method and Specht FEM were proposed for the simplest single layer model (1.4). For bilayer plates model (1.1), Kirchhoff FEM, IPDG, and local discontinuous Galerkin (LDG) methods have been designed in [8, 7, 9, 16, 18]. Moreover, LDG was devised for prestrained plates (1.6) in [14, 15]. We refer to [13] for a review article for a more thorough introduction.

Recently, a deep learning based method is designed in [26] for bilayer plates (1.1), and it utilizes a stochastic gradient descent method and deals with the constraint by adding a penalty term to the energy. Additionally, [34] incorporates the nonlinear metric constraint by Lagrange multipliers and solves the nonlinear problem via a Newton's method for a shell model similar to prestrained plates.

1.3. Accelerated gradient flows. Although the gradient flow type schemes are favored in existing works due to its easy-hands-on and computational stability, they converge slowly for difficult problems like bilayer plates, where the non-convexity brings a more significant challenge. Also, such gradient flow based algorithms are easily stuck at local minimizers for non-convex problems. With an attempt to overcome these limitations, we aim to design efficient and robust algorithms based on accelerated gradient flows for (1.1), (1.4) and (1.6) in this work.

The study of accelerated gradient flows can be traced back to the seminal Polyak's momentum method [33, 4] and also Nesterov's accelerated gradient descent method [30, 31] for convex optimization problems. More recently, an ODE interpretation of the Nesterov's method was established in [38], and inspired more advanced theoretical analysis and generalization; see for instance the works in [3, 2, 11, 22] and the references therein.

The investigation of these accelerated flows for scientific computing with real-world applications, which often involve non-convex variational models, is still in its early stages both theoretically and computationally. For instance, in [19], novel algorithms of accelerated flows show promising efficiency for computing ground states of Bose-Einstein condensate, although the paper lacks a thorough numerical analysis. Similarly, in [13, 12], a Nesterov type acceleration has been applied to the pre-asymptotic model of prestrained plates, which requires minimizing a non-convex energy without constraints and differs from the constrained minimization problem (1.6), resulting in effective reduction of computational time, yet an analysis remains open. Additionally, in [20], Nesterov's acceleration and the heavy ball method have been utilized for the Landau-de Gennes model of liquid crystals, demonstrating improved computational efficiency, but again numerical analysis is missing.

We develop novel accelerated algorithms for constrained minimization problems (1.1), (1.4), and (1.6) by integrating Nesterov's acceleration strategy and heavy ball method with the tangent space update strategy (1.9) that manages metric constraints. The accelerated flows entails modifying gradient flows (1.7) and (1.8) to be

$$(1.10) \quad \tau^{-2}(\delta \mathbf{y}^{n+1} + \mathbf{w}^n - \mathbf{y}^n) + \delta E[\delta \mathbf{y}^{n+1} + \mathbf{w}^n] = \mathbf{0}$$

for prestrained and single layer plates, and

$$(1.11) \quad \tau^{-2}(\delta \mathbf{y}^{n+1} + \mathbf{w}^n - \mathbf{y}^n) + \delta E_{bi}^c[\delta \mathbf{y}^{n+1} + \mathbf{w}^n] + \delta E_{bi}^{nc}[\mathbf{w}^n] = \mathbf{0}$$

for bilayer plates, where $\mathbf{w}^n := \mathbf{y}^n + \eta^n \delta \mathbf{y}^n$ is an auxiliary variable. η^n is a crucial coefficient that influences the acceleration effect and constraint violation. The choice $\eta^n = \frac{n-1}{n+\alpha-1}$ with $\alpha \geq 3$ corresponds to a generalized Nesterov's acceleration strategy, and $\eta^n = 1 - \beta\tau$ with $\beta > 0$ and $\beta\tau < 1$ corresponds to the heavy ball method. Moreover, we emphasize that in (1.10) and (1.11), $\delta \mathbf{y}^{n+1}$ is computed with the linearized constraint $L[\mathbf{y}^n; \delta \mathbf{y}^{n+1}] = \mathbf{0}$.

1.4. Contributions and outline of the paper. In section 2, we discuss a formal relation between our accelerated flow defined by (1.10) and a dissipative hyperbolic PDE involving second order time derivative of \mathbf{y} , which motivates us to prove monotone decreasing of a pseudo total energy which is the sum of $E = E_{pre}$ or E_{si} and a kinetic term. In contrast to gradient flows, E itself is oscillating in the accelerated flows, while the kinetic energy provably converges to 0 as $n \rightarrow \infty$. We show that the constraint violation is controlled by τ , at least in the same order as gradient flows. For bilayer plates, we prove the same results, the total energy stability and control of constraint violation, using an induction argument. In section 3, we extend our accelerated flows by further incorporating the backtracking/restarting strategy to guarantee a monotone decreasing of $E = E_{pre}$ (or E_{si} , E_{bi}), and a BDF2 approximation to seek a higher accuracy in constraint preservation. The latter is motivated by the recent work [1], where the BDF2 scheme was proposed to replace backward Euler in gradient flows with tangent space updates (1.9). All the proposed algorithms are tested with several benchmark examples, which not only verifies our theoretical

findings, but also illustrates the enhanced computational performance of the proposed methods.

The algorithms and theoretical discussions in this paper are presented with temporal semi-discrete formulations but hold verbatim if a general spatial discretization with certain consistency is considered. See our accompanying paper [21] for an example: we utilize Morley FEM to discretize spatially, and prove its convergence and consistency.

2. Accelerated gradient flows with tangent space update strategy: stability and admissibility. In this section, we present (temporal) semi-discrete formulations of accelerated gradient flows for constrained minimization problems (1.1), (1.4) and (1.6), and discuss its theoretical properties including energy stability and control of constraint violation. We first introduce some notations.

We fix the notations $\|\cdot\|_{L^p}$ ($1 \leq p \leq \infty$), $\|\cdot\|_{H^2}$, $|\cdot|_{H^2}$, $(\cdot, \cdot)_{L^2}$, and $(\cdot, \cdot)_{H^2}$ to represent norms, seminorms, and inner products on Sobolev spaces such as $L^p(\Omega)$ and $H^2(\Omega)$, as well as their vector-valued and tensor-valued counterparts. We will slightly abuse the inner product notation by defining $(\mathbf{v}, \mathbf{w})_{H^2} := (D^2\mathbf{v}, D^2\mathbf{w})_{L^2}$ whenever $\mathbf{v}, \mathbf{w} \in [H_0^2(\Omega)]^3$. This is indeed an inner product because $\|\mathbf{v}\|_{H^2} \approx |\mathbf{v}|_{H^2}$ holds for any $\mathbf{v} \in [H_0^2(\Omega)]^3$. Moreover, for simplicity of presentation, we assume $\Gamma^D \neq \emptyset$ in this work. Our analysis and method can be extended to free boundary conditions where $\Gamma^D = \emptyset$ in the spirit of [14, 15]. In this section, we use $C(\cdot)$ to represent generic constants, which are determined by the quantities in the parentheses. In particular, the use of the same $C(\cdot)$ indicates their dependence on the same data, but does not necessarily mean they are identical.

We will utilize the tangent space update strategy as described in Section 1.2, which results in a violation of constraint that we aim to control. Therefore, we define the violation $D_{g,p}$ with the given metric g and $1 \leq p \leq \infty$ and corresponding relaxed admissible sets $\mathcal{A}_{g,p}^\epsilon$ as

$$(2.1) \quad D_{g,p}[\mathbf{y}] := \|\mathbf{I}[\mathbf{y}] - g\|_{L^p},$$

and

$$(2.2) \quad \mathcal{A}_{g,p}^\epsilon := \{\mathbf{y} \in [H^2(\Omega)]^3 : D_{g,p}[\mathbf{y}] \leq \epsilon, \quad \mathbf{y} = \boldsymbol{\varphi}, \quad \nabla \mathbf{y} = \Phi \text{ on } \Gamma^D\}.$$

It is clear that in the limit of $\epsilon \rightarrow 0$ the metric constraints $\mathbf{I}[\mathbf{y}] = g$ are satisfied pointwise almost everywhere.

2.1. Prestrained plates. It is important to note that the models for prestrained and single layer plates have a similar structure: both the E_{pre} in (1.6) and E_{si} in (1.4) are convex, and the metric constraint (with different data) is imposed in both cases. Therefore, in this section, we discuss the accelerated flows for prestrained plates, which can be readily extended to single layer plates, after adding the force term as in (1.4). We define the bilinear form $a_g(\mathbf{y}, \mathbf{v}) := \delta E_{pre}[\mathbf{y}](\mathbf{v})$. For any $\mathbf{v} \in [H^2(\Omega)]^3$,

$$(2.3) \quad a_g(\mathbf{v}, \mathbf{v}) = 2E_{pre}[\mathbf{v}] \geq C(\lambda, \mu, g)|\mathbf{v}|_{H^2}^2.$$

Suppose we have a proper initial state $\mathbf{y}^0 \in \mathcal{A}_g$. At arbitrary n -th iteration ($n \geq 0$), we seek increments $\delta \mathbf{y}^{n+1} \in \mathcal{F}(\mathbf{y}^n)$, namely in the tangent space of metric constraint at \mathbf{y}^n , with the definition

$$(2.4) \quad \mathcal{F}(\mathbf{y}) := \{\mathbf{v} \in [H_0^2]^3 : L[\mathbf{y}; \mathbf{v}] = 0\}.$$

We now design the accelerated gradient flow, motivated by the seminal Nesterov's acceleration and heavy ball method in convex optimization [30, 38, 33, 4], though we are solving non-convex problems. Set $\mathbf{w}^0 = \mathbf{y}^0$, for any $n \geq 0$ we compute

$$(2.5) \quad \tau^{-2}(\delta \mathbf{y}^{n+1}, \mathbf{v})_{H^2} + a_g(\delta \mathbf{y}^{n+1}, \mathbf{v}) = -a_g(\mathbf{w}^n, \mathbf{v}) + \tau^{-2}(\mathbf{w}^n - \mathbf{y}^n, \mathbf{v})_{H^2}$$

$$(2.6) \quad \mathbf{y}^{n+1} = \mathbf{y}^n + \delta \mathbf{y}^{n+1}$$

$$(2.7) \quad \mathbf{w}^{n+1} = \mathbf{y}^{n+1} + \eta^{n+1} \delta \mathbf{y}^{n+1},$$

where η^n has two choices, namely $\eta^n = \frac{n-1}{n+\alpha-1}$ with $\alpha \geq 3$ (corresponding to Nesterov's acceleration), and $\eta^n = 1 - \beta\tau$ with $0 < \beta < 1/\tau$ (corresponding to the heavy ball method).

Cancelling \mathbf{w}^n in (2.5) and using that a_g is a bilinear form, we derive

$$\frac{1}{\tau^2}(\delta \mathbf{y}^{n+1}, \mathbf{v})_{H^2} + a_g(\delta \mathbf{y}^{n+1}, \mathbf{v}) = -a_g(\mathbf{y}^n, \mathbf{v}) - \eta^n a_g(\delta \mathbf{y}^n, \mathbf{v}) + \frac{\eta^n}{\tau^2}(\delta \mathbf{y}^n, \mathbf{v})_{H^2},$$

and then minus $\frac{1}{\tau^2}(\delta \mathbf{y}^n, \mathbf{v})_{H^2}$ on both sides and rearrange the terms to get

$$(2.8) \quad \frac{1}{\tau^2}(\delta \mathbf{y}^{n+1} - \delta \mathbf{y}^n, \mathbf{v})_{H^2} + \frac{1 - \eta^n}{\tau^2}(\delta \mathbf{y}^n, \mathbf{v})_{H^2} + a_g(\mathbf{y}^n, \mathbf{v}) + \eta^n a_g(\delta \mathbf{y}^n, \mathbf{v}) + a_g(\delta \mathbf{y}^{n+1}, \mathbf{v}) = 0.$$

Considering a continuous flow $Y(t, \mathbf{x}) \in C^2(0, \infty; [H^2(\Omega)]^3)$, we set $\mathbf{y}^n := Y(t_n, \cdot)$ with an arbitrary fixed $t_n > 0$, $n := t_n/\tau + \alpha - 1$ (τ is properly chosen to guarantee n is an integer) and $t_{n\pm 1} := t_n \pm \tau$. Using the Taylor expansion of $Y(t_{n+1}, \cdot)$ and $Y(t_{n-1}, \cdot)$ around $t = t_n$ in (2.8), noticing that $\frac{1-\eta^n}{\tau^2} = \frac{\alpha}{\tau t_n}$ when $\eta^n = \frac{n-1}{n+\alpha-1}$, and dropping $\mathcal{O}(\tau)$ terms for small enough τ yield the weak formulation of following PDE dynamics with artificial time $t = t_n$:

$$(2.9) \quad \ddot{Y}(t, \cdot) + \frac{\alpha}{t} \dot{Y}(t, \cdot) + \delta E_{pre}[Y(t, \cdot)] = 0.$$

We note that in this process the second line of (2.8) vanishes, because $|\eta^n| \leq 1$ and $\delta \mathbf{y}^n, \delta \mathbf{y}^{n+1} = \mathcal{O}(\tau)$. Separately, we can repeat the same formal asymptotic process in the constraint $\delta \mathbf{y}^{n+1} \in \mathcal{F}(\mathbf{y}^n)$, i.e., $(\nabla \delta \mathbf{y}^{n+1})^T \nabla \mathbf{y}^n + (\nabla \mathbf{y}^n)^T \nabla \delta \mathbf{y}^{n+1} = 0$, and drop the $\mathcal{O}(\tau^2)$ terms to obtain $\nabla \dot{Y}^T \nabla Y + \nabla Y^T \nabla \dot{Y} = 0$, namely $\frac{d(\nabla Y^T \nabla Y)}{dt} = 0$, which shows consistency to the metric constraint given $\nabla Y(0, \mathbf{x})^T \nabla Y(0, \mathbf{x}) = g(\mathbf{x})$. Moreover, when $\eta^n = 1 - \beta\tau$, the damping coefficient $\frac{\alpha}{t}$ in (2.9) is then replaced by a constant β , which is the form of heavy-ball dynamics as in [4].

A direct calculation implies that the PDE (2.9) guarantees the monotone decreasing of $\frac{1}{2} \|\dot{Y}(t, \cdot)\|^2 + E_{pre}[Y(t, \cdot)]$ along the flow $Y(t, \cdot)$. This motivates the following theorem.

THEOREM 2.1 (Total energy stability). *Suppose $n \geq 1$, $\mathbf{y}^n \in [H^2(\Omega)]^3$ and $\delta \mathbf{y}^n \in [H_0^2(\Omega)]^3$ are given, and $\delta \mathbf{y}^{n+1}$ is solved by (2.8). Define $\mathbf{y}^{n+1} := \mathbf{y}^n + \delta \mathbf{y}^{n+1}$. If $\tau \leq C(\lambda, \mu, g)^{-1/2}$ with the constant $C(\lambda, \mu, g)$ appearing in (2.3), then the following energy stability estimate is valid:*

$$(2.10) \quad E_{pre}[\mathbf{y}^{n+1}] + \frac{1}{2\tau^2} |\delta \mathbf{y}^{n+1}|_{H^2}^2 + \frac{1 - \eta^n}{2\tau^2} |\delta \mathbf{y}^{n+1}|_{H^2}^2 \leq E_{pre}[\mathbf{y}^n] + \frac{1}{2\tau^2} |\delta \mathbf{y}^n|_{H^2}^2.$$

Proof. Taking $\mathbf{v} = \delta \mathbf{y}^{n+1}$ in (2.8) and considering the following splittings

$$\begin{aligned}
 (2.11) \quad (\delta \mathbf{y}^{n+1} - \delta \mathbf{y}^n, \delta \mathbf{y}^{n+1})_{H^2} &= \frac{1}{2} \left(|\delta \mathbf{y}^{n+1}|_{H^2}^2 - |\delta \mathbf{y}^n|_{H^2}^2 + |\delta \mathbf{y}^{n+1} - \delta \mathbf{y}^n|_{H^2}^2 \right) \\
 a_g(\mathbf{y}^{n+1}, \delta \mathbf{y}^{n+1}) &= E_{pre}[\mathbf{y}^{n+1}] - E_{pre}[\mathbf{y}^n] + \frac{1}{2} a_g(\delta \mathbf{y}^{n+1}, \delta \mathbf{y}^{n+1}) \\
 (\delta \mathbf{y}^n, \delta \mathbf{y}^{n+1})_{H^2} &= \frac{1}{2} \left(|\delta \mathbf{y}^n|_{H^2}^2 + |\delta \mathbf{y}^{n+1}|_{H^2}^2 - |\delta \mathbf{y}^{n+1} - \delta \mathbf{y}^n|_{H^2}^2 \right) \\
 a_g(\delta \mathbf{y}^n, \delta \mathbf{y}^{n+1}) &= \frac{1}{2} \left(a_g(\delta \mathbf{y}^n, \delta \mathbf{y}^n) + a_g(\delta \mathbf{y}^{n+1}, \delta \mathbf{y}^{n+1}) \right) \\
 &\quad - \frac{1}{2} a_g(\delta \mathbf{y}^{n+1} - \delta \mathbf{y}^n, \delta \mathbf{y}^{n+1} - \delta \mathbf{y}^n),
 \end{aligned}$$

we derive

$$\begin{aligned}
 (2.12) \quad 0 &= \frac{1}{2\tau^2} \left(|\delta \mathbf{y}^{n+1}|_{H^2}^2 - |\delta \mathbf{y}^n|_{H^2}^2 \right) + E_{pre}[\mathbf{y}^{n+1}] - E_{pre}[\mathbf{y}^n] \\
 &\quad + \frac{1 - \eta^n}{2\tau^2} \left(|\delta \mathbf{y}^n|_{H^2}^2 + |\delta \mathbf{y}^{n+1}|_{H^2}^2 \right) + \frac{1 + \eta^n}{2} a_g(\delta \mathbf{y}^{n+1}, \delta \mathbf{y}^{n+1}) + \frac{\eta^n}{2} a_g(\delta \mathbf{y}^n, \delta \mathbf{y}^n) \\
 &\quad + \frac{\eta^n}{2\tau^2} |\delta \mathbf{y}^{n+1} - \delta \mathbf{y}^n|_{H^2}^2 - \frac{\eta^n}{2} a_g(\delta \mathbf{y}^{n+1} - \delta \mathbf{y}^n, \delta \mathbf{y}^{n+1} - \delta \mathbf{y}^n).
 \end{aligned}$$

Note that the first line gives the desired discrete total energy at \mathbf{y}^{n+1} and \mathbf{y}^n , and each term in the second line is non-negative as $0 \leq \eta^n < 1$ ($n \geq 1$). The third line is also non-negative after incorporating the coercivity estimate (2.3) and the assumption $\tau < C(\lambda, \mu, g)^{-1/2}$. This validates the energy stability (2.10). \square

Remark 2.1. Estimate (2.10) implies that the energy stability of the total energy $E_{pre}[\mathbf{y}^n] + \frac{1}{2\tau^2} |\delta \mathbf{y}^n|_{H^2}^2$, where the second term approximates $\frac{1}{2} \|\dot{\mathbf{Y}}\|_{H^2}^2$ and can be viewed as a kinetic energy. The term $\frac{1 - \eta^n}{2\tau^2} |\delta \mathbf{y}^{n+1}|_{H^2}^2$ in (2.10) is an energy dissipation term, which has other options, according to (2.12). We emphasize that the constant in the condition $\tau < C(\lambda, \mu, g)^{-1/2}$ is not affected by any discretization parameter and depends solely on the problem data. This condition is quite mild when the SPD matrix-valued g is bounded away from singular.

Moreover, as $\mathbf{w}^0 = \mathbf{y}^0$, taking $n = 0$ in (2.5) gives us a step of gradient flow with time-step τ^2 , and therefore we have the energy stability estimate [14]

$$(2.13) \quad E_{pre}[\mathbf{y}^1] + \frac{1}{\tau^2} |\delta \mathbf{y}^1|_{H^2}^2 \leq E_{pre}[\mathbf{y}^0].$$

Consequently, summing (2.10) over $n = 1$ to N for $N \geq 1$, considering telescopic cancellation and using $\eta^n = \frac{n-1}{n+\alpha-1}$ yield

$$(2.14) \quad E_{pre}[\mathbf{y}^{N+1}] + \frac{1}{2\tau^2} |\delta \mathbf{y}^{N+1}|_{H^2}^2 + \sum_{n=1}^N \frac{\alpha}{2(n+\alpha-1)\tau^2} |\delta \mathbf{y}^{n+1}|_{H^2}^2 \leq E_{pre}[\mathbf{y}^0].$$

Note that the RHS of (2.14) can still be considered as a total energy if one imposes zero velocity initial condition $\dot{\mathbf{Y}}(0, \cdot) = 0$ in (2.9). Moreover, when considering the choice of $\eta^n = 1 - \beta\tau$, the estimate (2.14) is valid upon replacing the coefficient $\frac{\alpha}{2(n+\alpha-1)\tau^2}$ by $\beta/(2\tau)$.

Since the total energy $E_{total}[\mathbf{y}^{n+1}] := E_{pre}[\mathbf{y}^{n+1}] + \frac{1}{2\tau^2} |\delta \mathbf{y}^{n+1}|_{H^2}^2$ is decreasing monotonically by Theorem 2.1, it is natural to stop the iterations when E_{total} stabilizes. Algorithm 2.1 summarizes the working procedure of the accelerated flows with

the choice of $\eta^n = \frac{n-1}{n+\alpha-1}$ (Nesterov's acceleration). An algorithm for the case with $\eta^n = 1 - \beta\tau$ merely requires an obvious and minor adjustment to Algorithm 2.1, which we will not repeat here for the sake of brevity.

Algorithm 2.1 Accelerated gradient flows.

- 1: Choose a pseudo time-step $\tau > 0$, a tolerance constant tol and parameter $\alpha \geq 3$.
 - 2: Choose initial guess $\mathbf{y}^0 \in \mathcal{A}_g$, set $\mathbf{w}^0 = \mathbf{y}^0$, $n = 0$ and $\Delta E_{\text{total}} = \infty$.
 - 3: **while** $\tau^{-1} \Delta E_{\text{total}} > \text{tol}$ **do**
 - 4: **Solve** (2.5) for $\delta \mathbf{y}^{n+1} \in \mathcal{F}(\mathbf{y}^n)$
 - 5: **Update** $\mathbf{y}^{n+1} = \mathbf{y}^n + \delta \mathbf{y}^{n+1}$, $\eta^{n+1} = \frac{n}{n+\alpha}$, $\mathbf{w}^{n+1} = \mathbf{y}^{n+1} + \eta^{n+1} \delta \mathbf{y}^{n+1}$
 - 6: **Set** $\Delta E_{\text{total}} = E_{\text{total}}[\mathbf{y}^{n+1}] - E_{\text{total}}[\mathbf{y}^n]$ and $n = n + 1$
 - 7: **end while**
 - 8: **return** \mathbf{y}^n
-

Based on the energy stability result, the limiting behaviour of the velocity term can be immediately derived, which is stated below.

COROLLARY 2.1. *Let $\{\mathbf{y}^n\}_{n \in \mathbb{N}}$ be the sequence produced in Algorithm 2.1 with a fixed $\tau > 0$, then the increments $\delta \mathbf{y}^{n+1} := \mathbf{y}^{n+1} - \mathbf{y}^n$ satisfy that $\liminf_{n \rightarrow \infty} |\delta \mathbf{y}^n|_{H^2} = 0$ when $\eta^n = \frac{n-1}{n+\alpha-1}$. When $\eta^n = 1 - \beta\tau$, the increments further satisfy that $\lim_{n \rightarrow \infty} |\delta \mathbf{y}^n|_{H^2} = 0$.*

Proof. When $\eta^n = \frac{n-1}{n+\alpha-1}$, (2.14) implies $\sum_{n=1}^N \frac{\alpha}{2(n+\alpha-1)\tau^2} |\delta \mathbf{y}^{n+1}|_{H^2}^2 \leq E_{\text{pre}}[\mathbf{y}^0]$ for all $N \in \mathbb{N}$ and every fixed $\tau > 0$. Taking $N \rightarrow \infty$, it is clear that for every fixed τ , $\frac{1}{\tau^2} \sum_{n=1}^{\infty} \frac{|\delta \mathbf{y}^n|_{H^2}^2}{n}$ is bounded. Therefore, we derive $\liminf_{n \rightarrow \infty} |\delta \mathbf{y}^n|_{H^2} = 0$.

When $\eta^n = 1 - \beta\tau$, then (2.14) implies $\frac{\beta}{2\tau} \sum_{n=1}^N |\delta \mathbf{y}^{n+1}|_{H^2}^2 \leq E_{\text{pre}}[\mathbf{y}^0]$ independent of N . This shows that $\lim_{n \rightarrow \infty} |\delta \mathbf{y}^n|_{H^2} = 0$ for every fixed $\tau > 0$. \square

The metric constraint $\mathbb{I}[\mathbf{y}] = g$ is not imposed exactly in the flow, because we only require $\delta \mathbf{y}^{n+1} \in \mathcal{F}(\mathbf{y}^n)$. Next, we provide an estimate on the control of the violation of metric constraint to justify the admissibility of \mathbf{y}^{N+1} in $\mathcal{A}_{g,1}^\epsilon$ for any $N \geq 0$.

THEOREM 2.2 (Admissibility). *Suppose $\mathbf{y}^0 \in \mathcal{A}_g$. Let \mathbf{y}^{N+1} be any iterate in Algorithm 2.1, $N \geq 0$ and $\tau \leq C(\lambda, \mu, g)^{-1/2}$ with the constant $C(\lambda, \mu, g)$ appearing in (2.3). Then $\mathbf{y}^{N+1} \in \mathcal{A}_{g,1}^\epsilon$ with $\epsilon = C(\Omega, \alpha)N\tau^2 E_{\text{pre}}[\mathbf{y}^0]$.*

Proof. Using the tangent plane constraint $\delta \mathbf{y}_h^{n+1} \in \mathcal{F}(\mathbf{y}_h^n)$, a Poincaré-type inequality for $\delta \mathbf{y}_h^{n+1} \in [H_0^2(\Omega)]^3$ and telescopic cancellation, we derive

$$(2.15) \quad \|\mathbb{I}[\mathbf{y}^{N+1}] - g\|_{L^1(\Omega)} \leq \|\mathbb{I}[\mathbf{y}^0] - g\|_{L^1(\Omega)} + C(\Omega) \sum_{n=0}^N |\delta \mathbf{y}_h^{n+1}|_{H^2}^2.$$

Assuming $N \geq 1$ and resorting to (2.14), we compute

$$(2.16) \quad \frac{\alpha}{2(N+\alpha-1)\tau^2} \sum_{n=1}^N |\delta \mathbf{y}^{n+1}|_{H^2}^2 < \sum_{n=1}^N \frac{\alpha}{2(n+\alpha-1)\tau^2} |\delta \mathbf{y}^{n+1}|_{H^2}^2 \leq E_{\text{pre}}[\mathbf{y}^0],$$

and together with (2.13) we conclude that for $N \geq 1$

$$\|\mathbb{I}[\mathbf{y}^{N+1}] - g\|_{L^1(\Omega)} \leq C(\Omega) \left(1 + \frac{2(N+\alpha-1)}{\alpha}\right) \tau^2 E_{\text{pre}}[\mathbf{y}^0] \leq C(\Omega, \alpha) N \tau^2 E_{\text{pre}}[\mathbf{y}^0],$$

where $C(\Omega, \alpha)$ is a constant that guarantees $C(\Omega, \alpha)N > C(\Omega)(1 + \frac{2(N+\alpha-1)}{\alpha})$ for $N \geq 1$ with $C(\Omega)$ appearing in (2.15). Moreover, if $N = 0$, (2.15) and (2.13) yield

$$(2.17) \quad \|I[\mathbf{y}^1] - g\|_{L^1(\Omega)} \leq C(\Omega)\tau^2 E_{pre}[\mathbf{y}^0] < C(\Omega, \alpha)N\tau^2 E_{pre}[\mathbf{y}^0].$$

Taking $\epsilon := C(\Omega, \alpha)N\tau^2 E_{pre}[\mathbf{y}^0]$ concludes the proof. \square

Remark 2.2. At a first glance, the constraint violation given in Theorem 2.2 may seem problematic, as the control parameter ϵ is not uniform and depends on iteration numbers. However, by employing the stopping criteria in Algorithm 2.1, it is consistently observed that the total number of iterations $N = \mathcal{O}(\tau^{-1})$ in numerical simulations in Section 3.3. Specifically, recalling $E_{total}[\mathbf{y}^{n+1}] := E_{pre}[\mathbf{y}^{n+1}] + \frac{1}{2\tau^2}|\delta\mathbf{y}^{n+1}|_{H^2}^2$, and given $\text{tol} > 0$, the iteration is terminated at the N -th step if

$$(2.18) \quad \tau^{-1}(E_{total}[\mathbf{y}^{N-1}] - E_{total}[\mathbf{y}^N]) < \text{tol}.$$

We resort to the continuous second-order dynamics in (2.9) for a formal explanation of $N = \mathcal{O}(\tau^{-1})$. Since our scheme can be asymptotically viewed as a temporal discretization of (2.9), we can establish a connection between the iteration number and the terminal time T of the continuous dynamics as $T = N\tau$. On the continuous level, the practical stopping criteria (2.18) can be interpreted as

$$(2.19) \quad \left| \frac{d}{dt} \left(\frac{1}{2} \|\dot{Y}\|^2 + E_{pre}[Y] \right) \right| < \text{tol}.$$

It is evident from (2.9) that $\lim_{t \rightarrow \infty} \frac{d}{dt} \left(\frac{1}{2} \|\dot{Y}\|^2 + E_{pre}[Y] \right) = 0$, ensuring the existence of $T(\text{tol}) > 0$, depending on the fixed $\text{tol} > 0$, such that (2.19) is satisfied. Consequently, on the discrete level, $N = T(\text{tol})\tau^{-1} = \mathcal{O}(\tau^{-1})$.

Returning to Theorem 2.2, we can refine the estimate of constraint violation so that $\mathbf{y}^N \in \mathcal{A}_{g,1}^\epsilon$ with $\epsilon = C(\Omega, \alpha, \text{tol})\tau E_{pre}[\mathbf{y}^0]$. In Section 3.3, all numerical experiments confirm that the constraint violation is of order $\mathcal{O}(\tau)$ and the constant $C(\Omega, \alpha, \text{tol})$ stabilizes as $\text{tol} \rightarrow 0$ (so does the constraint violation).

Moreover, if we use $\eta^n = 1 - \beta\tau$ (heavy ball method) in Algorithm 2.1, it will be straightforward to conclude that $\mathbf{y}^N \in \mathcal{A}_{g,1}^\epsilon$ with $\epsilon = C(\Omega, \beta)\tau E_{pre}[\mathbf{y}^0]$.

2.2. Bilayer plates. We first discuss the coercivity of E_{bi} for bilayer plates. In fact, it is obviously coercive when \mathbf{y} satisfies $\nabla \mathbf{y}^T \nabla \mathbf{y} = I_2$ exactly. However, since this isometry constraint is not kept in our algorithms, we need to show coercivity under a relaxed constraint for $\mathbf{y} \in \mathcal{A}_{I_2,2}^\epsilon$. Here, the use of L^2 norm is critical to estimate the cubic term E_{bi}^{nc} ; L^1 norm seems to be not enough.

THEOREM 2.3 (Coercivity). *Let $\epsilon > 0$ and $\mathbf{y} \in \mathcal{A}_{I_2,2}^\epsilon$. There exists a positive constant $C(\Omega)$ such that*

$$(2.20) \quad \|\mathbf{y}\|_{H^2}^2 \leq C(\Omega) \left(E_{bi}[\mathbf{y}] + C(\boldsymbol{\varphi}, \Phi) + (\epsilon^2 + 2|\Omega|) \|Z\|_{L^\infty}^2 \right).$$

Proof. We first note that

$$(2.21) \quad \|\nabla \mathbf{y}\|_{L^4}^4 \leq 2\|\nabla \mathbf{y}^T \nabla \mathbf{y}\|_{L^2}^2 \leq 4(\|\nabla \mathbf{y}^T \nabla \mathbf{y} - I_2\|_{L^2}^2 + \|I_2\|_{L^2}^2) = 4(\epsilon^2 + 2|\Omega|).$$

Using (2.21), Hölder inequality and Cauchy inequality, we estimate

$$\begin{aligned}
(2.22) \quad |\mathbf{y}|_{H^2}^2 &= 2E_{bi}[\mathbf{y}] + 2 \sum_{i,j=1}^2 \int_{\Omega} \partial_{ij} \mathbf{y} \cdot (\partial_1 \mathbf{y} \times \partial_2 \mathbf{y}) Z_{ij} \\
&\leq 2E_{bi}[\mathbf{y}] + 4|\mathbf{y}|_{H^2} \|\nabla \mathbf{y}\|_{L^4}^2 \|Z\|_{L^\infty} \\
&\leq 2E_{bi}[\mathbf{y}] + 32(\epsilon^2 + 2|\Omega|) \|Z\|_{L^\infty}^2 + \frac{1}{2} |\mathbf{y}|_{H^2}^2.
\end{aligned}$$

Then, incorporating the Poincaré inequality $\|\mathbf{y}\|_{H^2}^2 \leq C(\Omega)(|\mathbf{y}|_{H^2}^2 + C(\varphi, \Phi))$ we conclude the proof. \square

For any $\mathbf{y} \in [H^2(\Omega)]^3$, we define $\ell[\mathbf{y}](\cdot) := \delta E_{bi}^{nc}[\mathbf{y}](\cdot)$, namely

$$(2.23) \quad \ell[\mathbf{y}](\mathbf{v}) := \sum_{i,j=1}^2 \int_{\Omega} \left(\partial_{ij} \mathbf{v} \cdot (\partial_1 \mathbf{y} \times \partial_2 \mathbf{y}) + \partial_{ij} \mathbf{y} \cdot (\partial_1 \mathbf{v} \times \partial_2 \mathbf{y} + \partial_1 \mathbf{y} \times \partial_2 \mathbf{v}) \right) Z_{ij}.$$

Moreover, by Sobolev embedding of H^1 into L^4 and Hölder inequality, for any $\mathbf{v} \in [H_0^2(\Omega)]^3$ the following estimate is valid:

$$(2.24) \quad |\ell[\mathbf{y}](\mathbf{v})| \leq C(\Omega, Z) |\mathbf{v}|_{H^2} \|\mathbf{y}\|_{H^2}^2.$$

We next discuss an accelerated gradient flow for bilayer plates. It is the same as Algorithm 2.1, except that $\delta \mathbf{y}^{n+1}$ is now computed by (2.25) instead of (2.5). The iteration is also terminated with the condition (2.18), upon replacing E_{pre} by E_{bi} in the definition of E_{total} .

More specifically, motivated by the gradient flow in [18], we consider an explicit treatment of E_{bi}^{nc} so that the ensuing problem is linear. Given $\mathbf{y}^0 \in \mathcal{A}$, set $\mathbf{w}^0 = \mathbf{y}^0$, and we compute the increment $\delta \mathbf{y}^{n+1} \in \mathcal{F}(\mathbf{y}^n)$ in each iteration and update by

$$(2.25) \quad \tau^{-2}(\delta \mathbf{y}^{n+1}, \mathbf{v})_{H^2} + a(\delta \mathbf{y}^{n+1}, \mathbf{v}) = \ell[\mathbf{w}^n](\mathbf{v}) - a(\mathbf{w}^n, \mathbf{v}) + \tau^{-2}(\mathbf{w}^n - \mathbf{y}^n, \mathbf{v})_{H^2}$$

$$(2.26) \quad \mathbf{y}^{n+1} = \mathbf{y}^n + \delta \mathbf{y}^{n+1}$$

$$(2.27) \quad \mathbf{w}^{n+1} = \mathbf{y}^{n+1} + \eta^{n+1} \delta \mathbf{y}^{n+1},$$

where $\eta^n = \frac{n-1}{n+\alpha-1}$ or $\eta^n = 1 - \beta\tau$. Here, $a(\mathbf{y}, \mathbf{v}) := \int_{\Omega} D^2 \mathbf{y} : D^2 \mathbf{v}$. Similar to (2.8), we rewrite (2.25) as

$$\begin{aligned}
(2.28) \quad \frac{1}{\tau^2}(\delta \mathbf{y}^{n+1} - \delta \mathbf{y}^n, \mathbf{v})_{H^2} + \frac{1 - \eta^n}{\tau^2}(\delta \mathbf{y}^n, \mathbf{v})_{H^2} + a(\mathbf{y}^n, \mathbf{v}) - \ell[\mathbf{w}^n](\mathbf{v}) \\
+ \eta^n a(\delta \mathbf{y}^n, \mathbf{v}) + a(\delta \mathbf{y}^{n+1}, \mathbf{v}) = 0.
\end{aligned}$$

We can further replace $\ell[\mathbf{w}^n](\mathbf{v})$ in (2.28) by $\ell[\mathbf{y}^n](\mathbf{v})$ after introducing the remainder $R^n(\mathbf{v})$, which is defined as

$$(2.29) \quad R^n(\mathbf{v}) := \ell[\mathbf{w}^n](\mathbf{v}) - \ell[\mathbf{y}^n](\mathbf{v}).$$

Substituting back to (2.28), we get

$$\begin{aligned}
(2.30) \quad \frac{1}{\tau^2}(\delta \mathbf{y}^{n+1} - \delta \mathbf{y}^n, \mathbf{v})_{H^2} + \frac{1 - \eta^n}{\tau^2}(\delta \mathbf{y}^n, \mathbf{v})_{H^2} + a(\mathbf{y}^n, \mathbf{v}) - \ell[\mathbf{y}^n](\mathbf{v}) \\
+ \eta^n a(\delta \mathbf{y}^n, \mathbf{v}) + a(\delta \mathbf{y}^{n+1}, \mathbf{v}) = R^n(\mathbf{v}).
\end{aligned}$$

We next estimate the remainder $R^n(\mathbf{v})$, which will be useful in the proof of stability.

LEMMA 2.3 (Estimate of remainder). *The following estimate holds for $R^n(\mathbf{v})$ defined by (2.29) and any $\mathbf{v} \in [H_0^2(\Omega)]^3$:*

$$(2.31) \quad |R^n(\mathbf{v})| \leq C(\Omega, Z) \left(|\mathbf{v}|_{H^2} |\delta \mathbf{y}^n|_{H^2} \left(|\mathbf{y}^n|_{H^2} + C(\boldsymbol{\varphi}, \Phi) \right) + |\mathbf{v}|_{H^2} |\delta \mathbf{y}^n|_{H^2}^2 \right).$$

Proof. Substituting the definition of \mathbf{w}^n in (2.27) into the expression (2.23) of linear functional ℓ and calculating the difference in (2.29), we can explicitly express R^n as a sum of several integrals involving $\mathbf{v}, \mathbf{y}^n, \delta \mathbf{y}^n$. Here, we drop the tedious expression, while the calculation is straightforward. We then estimate each term by using Hölder inequality, Poincaré inequality, the embedding of $H^1(\Omega)$ into $L^4(\Omega)$, and the fact that $|\eta^n| < 1$, to arrive at (2.31). \square

Note that as $\mathbf{w}^0 = \mathbf{y}^0$, taking $n = 0$ in (2.5) gives us a step of gradient flow with time-step τ^2 , and therefore we have the energy stability estimate [18]

$$(2.32) \quad E_{bi}[\mathbf{y}^1] + \frac{1}{2\tau^2} |\delta \mathbf{y}^1|_{H^2}^2 \leq E_{bi}[\mathbf{y}^0].$$

THEOREM 2.4 (Total energy stability). *Let $\mathbf{y}^0 \in \mathcal{A}$ and $M = 1, \dots, N-1$ be the iteration number of accelerated flow defined by (2.25), (2.26), and (2.27) with $\eta^n = \frac{n-1}{n+\alpha-1}$, where N is the total number of iterations when the accelerated flow is stopped by the criterion in Remark 2.2 and we assume $N = \alpha_0 \tau^{-1}$ with a constant $\alpha_0 > 0$. There exists a constant $\alpha_1 = \alpha_1(\mathbf{y}^0, \boldsymbol{\varphi}, \Phi, Z, \Omega, \alpha, \alpha_0) > 0$ independent of M such that if $\tau < \alpha_1$, then the following energy stability estimate is valid:*

$$(2.33) \quad \frac{1}{2\tau^2} |\delta \mathbf{y}^{M+1}|_{H^2}^2 + E_{bi}[\mathbf{y}^{M+1}] + \frac{1-\eta^M}{4\tau^2} \left(|\delta \mathbf{y}^{M+1}|_{H^2}^2 + |\delta \mathbf{y}^M|_{H^2}^2 \right) \leq \frac{1}{2\tau^2} |\delta \mathbf{y}^M|_{H^2}^2 + E_{bi}[\mathbf{y}^M].$$

In addition, there exists $\alpha_2 = \alpha_2(\Omega, \alpha, \alpha_0) > 0$, independent of M , such that

$$(2.34) \quad D_{I_2,2}[\mathbf{y}^{M+1}] \leq \alpha_2 \tau E_{bi}[\mathbf{y}^0].$$

Proof. We proceed by an induction argument. We first note that it is straightforward to verify (2.33) and (2.34) for $M = 1$ by a direct calculation.

We next assume (2.33) and (2.34) hold for $M = 1, \dots, n-1$ for $2 \leq n \leq N-1$. Then our goal is to prove the same estimates for $M = n$.

Step (i), intermediate estimate. Taking $\mathbf{v} = \delta \mathbf{y}^{n+1}$ in (2.30) and using the same splittings as in (2.11), we derive

$$(2.35) \quad \begin{aligned} & \frac{1}{2\tau^2} \left(|\delta \mathbf{y}^{n+1}|_{H^2}^2 - |\delta \mathbf{y}^n|_{H^2}^2 \right) + \frac{1}{2} a(\mathbf{y}^{n+1}, \mathbf{y}^{n+1}) - \frac{1}{2} a(\mathbf{y}^n, \mathbf{y}^n) \\ & + \frac{1-\eta^n}{2\tau^2} \left(|\delta \mathbf{y}^n|_{H^2}^2 + |\delta \mathbf{y}^{n+1}|_{H^2}^2 \right) + \frac{1+\eta^n}{2} a(\delta \mathbf{y}^{n+1}, \delta \mathbf{y}^{n+1}) + \frac{\eta^n}{2} a(\delta \mathbf{y}^n, \delta \mathbf{y}^n) \\ & + \frac{\eta^n}{2\tau^2} |\delta \mathbf{y}^{n+1} - \delta \mathbf{y}^n|_{H^2}^2 - \frac{\eta^n}{2} a(\delta \mathbf{y}^{n+1} - \delta \mathbf{y}^n, \delta \mathbf{y}^{n+1} - \delta \mathbf{y}^n) \\ & = \ell[\mathbf{y}^n](\delta \mathbf{y}^{n+1}) + R^n(\delta \mathbf{y}^{n+1}). \end{aligned}$$

Recalling $a(\mathbf{y}, \mathbf{y}) = |\mathbf{y}|_{H^2}^2$, $0 < \eta^n < 1$, and taking $\tau < 1$, it is clear that the second and third lines both are non-negative. Therefore, (2.35) becomes

$$(2.36) \quad \frac{1}{2\tau^2} |\delta \mathbf{y}^{n+1}|_{H^2}^2 + \frac{1}{2} |\mathbf{y}^{n+1}|_{H^2}^2 \leq \frac{1}{2\tau^2} |\delta \mathbf{y}^n|_{H^2}^2 + \frac{1}{2} |\mathbf{y}^n|_{H^2}^2 + \ell[\mathbf{y}^n](\delta \mathbf{y}^{n+1}) + R^n(\delta \mathbf{y}^{n+1}).$$

To control the right hand side, we use induction assumption and (2.32) to yield

$$\frac{1}{2\tau^2} |\delta \mathbf{y}^n|_{H^2}^2 + E_{bi}[\mathbf{y}^n] \leq \frac{1}{2\tau^2} |\delta \mathbf{y}^1|_{H^2}^2 + E_{bi}[\mathbf{y}^1] \leq E_{bi}[\mathbf{y}^0].$$

We note that $\mathbf{y}^n \in \mathcal{A}_{I_2,2}^\epsilon$ with $\epsilon = \alpha_1 \alpha_2 E_{bi}[\mathbf{y}^0]$ as (2.34) holds for $M = n$ and $\tau < \alpha_1$. Then resorting to Theorem 2.3 (coercivity) and requiring $\alpha_1 \leq 1$, we derive

$$(2.37) \quad \frac{1}{2\tau^2} |\delta \mathbf{y}^n|_{H^2}^2 + \frac{1}{2} |\mathbf{y}^n|_{H^2}^2 \leq C(\mathbf{y}^0, Z, \Omega) \alpha_2^2 + C(\mathbf{y}^0, \boldsymbol{\varphi}, \Phi, Z, \Omega).$$

Therefore, substituting (2.37) into the RHS of (2.36), combining with estimates (2.31) and (2.24) for $R^n(\delta \mathbf{y}^{n+1})$ and $\ell[\mathbf{y}^n](\delta \mathbf{y}^{n+1})$, and then using Cauchy inequality to produce $\frac{1}{2} |\delta \mathbf{y}^{n+1}|_{H^2}^2$ on the RHS of (2.36), we obtain an intermediate estimate:

$$(2.38) \quad \begin{aligned} & \left(\frac{1}{2\tau^2} - \frac{1}{2} \right) |\delta \mathbf{y}^{n+1}|_{H^2}^2 + \frac{1}{2} |\mathbf{y}^{n+1}|_{H^2}^2 \\ & \leq C(\mathbf{y}^0, Z, \Omega) \alpha_2^4 + C(\mathbf{y}^0, \boldsymbol{\varphi}, \Phi, Z, \Omega) \alpha_2^2 + C(\mathbf{y}^0, \boldsymbol{\varphi}, \Phi, Z, \Omega), \end{aligned}$$

and we emphasize that the constants $C(\mathbf{y}^0, Z, \Omega)$, $C(\mathbf{y}^0, \boldsymbol{\varphi}, \Phi, Z, \Omega)$ in (2.37) and (2.38) are generic and not necessarily the same, but they depend on the same data specified within the parentheses.

Step (ii), energy stability estimate. Using the algebraic relation

$$\begin{aligned} & (a^{M+1} - a^M) b^M c^M + a^M (b^{M+1} - b^M) c^M + a^M b^M (c^{M+1} - c^M) \\ & = a^{M+1} b^{M+1} c^{M+1} - a^M b^M c^M - (a^{M+1} - a^M) (b^{M+1} - b^M) c^{M+1} \\ & \quad - (a^{M+1} - a^M) b^M (c^{M+1} - c^M) - a^M (b^{M+1} - b^M) (c^{M+1} - c^M), \end{aligned}$$

we rewrite $\ell[\mathbf{y}^n](\delta \mathbf{y}^{n+1})$ as follows:

$$(2.39) \quad \begin{aligned} \ell[\mathbf{y}^n](\delta \mathbf{y}^{n+1}) &= \sum_{i,j=1}^2 \int_{\Omega} (\partial_{ij} \mathbf{y}^{n+1} \cdot (\partial_1 \mathbf{y}^{n+1} \times \partial_2 \mathbf{y}^{n+1}) - \partial_{ij} \mathbf{y}^n \cdot (\partial_1 \mathbf{y}^n \times \partial_2 \mathbf{y}^n)) Z_{ij} \\ &\quad - \sum_{i,j=1}^2 \int_{\Omega} \partial_{ij} \delta \mathbf{y}^{n+1} \cdot (\partial_1 \delta \mathbf{y}^{n+1} \times \partial_2 \mathbf{y}^{n+1} + \partial_1 \mathbf{y}^n \times \partial_2 \delta \mathbf{y}^{n+1}) Z_{ij} \\ &\quad - \sum_{i,j=1}^2 \int_{\Omega} \partial_{ij} \mathbf{y}^n \cdot (\partial_1 \delta \mathbf{y}^{n+1} \times \partial_2 \delta \mathbf{y}^{n+1}) Z_{ij}. \end{aligned}$$

Substituting this into (2.35), we note that the terms in first line are exactly the cubic energies $E_{bi}^{nc}[\mathbf{y}^{n+1}]$, $E_{bi}^{nc}[\mathbf{y}^n]$ and contribute to the full energies $E_{bi}[\mathbf{y}^{n+1}]$, $E_{bi}[\mathbf{y}^n]$. In contrast, the remaining terms must be estimated and absorbed into terms involved $|\delta \mathbf{y}^n|_{H^2}^2 + |\delta \mathbf{y}^{n+1}|_{H^2}^2$ in the second line of (2.35). To this end, we estimate and obtain

$$\begin{aligned} & \frac{1}{2\tau^2} (|\delta \mathbf{y}^{n+1}|_{H^2}^2 - |\delta \mathbf{y}^n|_{H^2}^2) + E_{bi}[\mathbf{y}^{n+1}] - E_{bi}[\mathbf{y}^n] + \frac{1 - \eta^n}{2\tau^2} (|\delta \mathbf{y}^{n+1}|_{H^2}^2 + |\delta \mathbf{y}^n|_{H^2}^2) \\ & \leq C(\Omega, Z) |\delta \mathbf{y}^{n+1}|_{H^2}^2 \left(|\mathbf{y}^{n+1}|_{H^2} + |\mathbf{y}^n|_{H^2} + C(\boldsymbol{\varphi}, \Phi) \right) \\ & \quad + C(\Omega, Z) \left(|\delta \mathbf{y}^{n+1}|_{H^2} |\delta \mathbf{y}^n|_{H^2} (|\mathbf{y}^n|_{H^2} + C(\boldsymbol{\varphi}, \Phi)) + |\delta \mathbf{y}^{n+1}|_{H^2} |\delta \mathbf{y}^n|_{H^2}^2 \right) \\ & \leq f_1(\alpha_2) |\delta \mathbf{y}^{n+1}|_{H^2}^2 + f_2(\alpha_2) |\delta \mathbf{y}^n|_{H^2}^2, \end{aligned}$$

For the first inequality we have used Hölder inequality, embedding of H^1 into L^4 , and Poincaré inequality to estimate the second and third line of (2.39), and used (2.31) to estimate $R^n(\delta \mathbf{y}^{n+1})$. For the second inequality, we use intermediate estimate (2.37) and (2.38). The constants $f_1(\alpha_2)$, $f_2(\alpha_2)$ are polynomials of $\alpha_2 > 0$ with coefficients $C(\mathbf{y}^0, \boldsymbol{\varphi}, \Phi, Z, \Omega) > 0$ depending only on the problem data and independent of n , and thus they are monotonically increasing as α_2 increases.

Our next goal is to find α_1 such that when $\tau < \alpha_1$ the following estimate is valid:

$$(2.40) \quad f_1(\alpha_2)|\delta \mathbf{y}^{n+1}|_{H^2}^2 + f_2(\alpha_2)|\delta \mathbf{y}^n|_{H^2}^2 \leq \frac{1-\eta^n}{4\tau^2} \left(|\delta \mathbf{y}^{n+1}|_{H^2}^2 + |\delta \mathbf{y}^n|_{H^2}^2 \right).$$

We note that $1 - \eta^n \geq 1 - \frac{N-1}{N+\alpha-1}$. Exploiting the assumption $N = \alpha_0\tau^{-1}$, we derive $\frac{1-\eta^n}{4\tau^2} \geq \frac{\alpha}{4(\alpha_0\tau+(\alpha-1)\tau^2)}$. As $\alpha_0 > 0$, $\alpha > 1$, $f_1(\alpha_2), f_2(\alpha_2) > 0$, we can conclude (2.40) when $\max\{f_1(\alpha_2), f_2(\alpha_2)\} \leq \frac{\alpha}{4(\alpha_0\tau+(\alpha-1)\tau^2)}$ from which we infer $\tau < \frac{-\alpha_0 + \sqrt{\alpha_0^2 + \alpha(\alpha-1)/\max\{f_1(\alpha_2), f_2(\alpha_2)\}}}{2(\alpha-1)}$. Recall that we have required $\alpha_1 \leq 1$. This leads to the choice

$$\alpha_1 := \min \left\{ 1, \frac{-\alpha_0 + \sqrt{\alpha_0^2 + \alpha(\alpha-1)/\max\{f_1(\alpha_2), f_2(\alpha_2)\}}}{2(\alpha-1)} \right\},$$

and α_1 depends on $\mathbf{y}^0, \varphi, \Phi, Z, \Omega, \alpha, \alpha_0$. Subsequently, (2.40) further leads to the desired estimate (2.33) for $M = n$.

Step (iii), control of constraint violation. It remains to verify (2.34) for $M = n$. Exploiting $\delta \mathbf{y}^{M+1} \in \mathcal{F}(\mathbf{y}^M)$, we derive

$$D_{I_2,2}[\mathbf{y}^{M+1}] \leq D_{I_2,2}[\mathbf{y}^M] + \|\mathbf{I}[\delta \mathbf{y}^{M+1}]\|_{L^2(\Omega)}.$$

Summing over $M = 0, \dots, n$, using telescopic cancellation, considering Hölder inequality and embedding of H^1 into L^4 , and recalling $\mathbf{y}^0 \in \mathcal{A}$, we obtain

$$D_{I_2,2}[\mathbf{y}^{n+1}] \leq C(\Omega) \sum_{k=0}^n |\delta \mathbf{y}^{k+1}|_{H^2}^2.$$

Summing (2.33) over $M = 1, \dots, n$, using (2.32), $\eta^M = \frac{M-1}{M+\alpha-1}$ and $n \leq N$, we obtain

$$D_{I_2,2}[\mathbf{y}^{n+1}] \leq C(\Omega, \alpha) N \tau^2 E_{bi}[\mathbf{y}^0].$$

Recalling $N = \alpha_0\tau^{-1}$, this finishes the proof of (2.34) for $M = n$ when $\alpha_2 > C(\Omega, \alpha)\alpha_0$. Upon fixing α_2 , it provides a uniform choice (independent of M) of constants in the induction argument. This concludes the proof. \square

When $\eta^n = 1 - \beta\tau$, we can readily obtain the stability and control of constraint violation as Theorem 2.4 with simpler details and without the need for the assumption $N = \alpha_0\tau^{-1}$. For brevity, we omit restating the statement and proof.

The energy stability of both prestrained and bilayer plates results in the convergence of iterates generated in accelerated flows as an immediate consequence.

COROLLARY 2.2. *Let $\{\mathbf{y}^n\}_{n \in \mathbb{N}}$ be a sequence produced in Algorithm 2.1 either for prestrained or bilayer plates, then there exists a convergent subsequence in $[H^1(\Omega)]^3$.*

Proof. Due to the coercivity (2.3) and (2.20) of both the energy functionals and the energy stability, we derive the uniform bounds on the sequence such that

$$\|\mathbf{y}^n\|_{H^2(\Omega)} \leq C(\Omega, \mathbf{y}^0, Z, \varphi, \Phi, g, \lambda, \mu) \quad \text{for all } n \in \mathbb{N}.$$

Here $C(\Omega, \mathbf{y}^0, Z, \varphi, \Phi, g, \lambda, \mu)$ is a constant with dependence of data covering both cases of prestrained and bilayer plates. This shows that there exists a weakly convergent subsequence in $[H^2(\Omega)]^3$ and a convergent subsequence in $[H^1(\Omega)]^3$, upon using the compact embedding of $H^2(\Omega)$ in $H^1(\Omega)$. \square

3. Variations of algorithms, computations, and numerical results. In this section, we provide the numerical aspects related to the accelerated flows. We first introduce some variants of Algorithm 2.1, which show interesting outreach of the accelerated flows. A short description of the space discretization using the Morley FEM [29, 39] is provided, though a detailed analysis of the fully discretized scheme will be presented in our accompanying paper [21]. Numerical examples to illustrate the performance of our accelerated flow algorithms are documented, which not only verify our theoretical results, but also demonstrate the significant improvements over existing methods.

3.1. Variations of accelerated flows. In this part, we present variations of Algorithm 2.1, where we combine other strategies with accelerated flows. These variations can further improve computational performance as illustrated in Section 3.3 in terms of efficiency or accuracy.

3.1.1. Backtracking and restarting. It is important to note that Algorithm 2.1 cannot guarantee a monotonically decreasing of potential energies $E = E_{pre}$ (resp. E_{bi}). However, we can further adopt a backtracking and restarting strategy in Algorithm 2.1 whenever the potential energy increases. The modified algorithm is presented in Algorithm 3.1.

Algorithm 3.1 Accelerated flow with backtracking and restarting strategy

```

1: Given a pseudo time-step  $\tau > 0$ , a tolerance  $tol$  and parameter  $\alpha \geq 3$ 
2: Choose  $\mathbf{y}^0 \in \mathcal{A}$ , set  $\mathbf{w}^0 = \mathbf{y}^0$ ,  $n = 0$ ,  $k = 0$  and  $\Delta E_{total} = \infty$ 
3: while  $\tau^{-1} \Delta E_{total} > tol$  do
4:   Solve (2.5) (resp. (2.25)) for  $\delta \mathbf{y}^{n+1} \in \mathcal{F}(\mathbf{y}^n)$ 
5:   Update  $\mathbf{y}^{n+1} = \mathbf{y}^n + \delta \mathbf{y}^{n+1}$ 
6:   Set  $\Delta E_{total} = E_{total}[\mathbf{y}^{n+1}] - E_{total}[\mathbf{y}^n]$  and  $\Delta E = E[\mathbf{y}^{n+1}] - E[\mathbf{y}^n]$ 
7:   if  $\Delta E < 0$  then
8:     Set  $k = k + 1$ 
9:   else
10:    Backtrack  $\mathbf{y}^{n+1} = \mathbf{y}^n$ 
11:    Restart  $k = 1$ 
12:  end if
13:  Update  $\eta^{n+1} = \frac{k-1}{k-1+\alpha}$  and  $\mathbf{w}^{n+1} = \mathbf{y}^{n+1} + \eta^{n+1} \delta \mathbf{y}^{n+1}$ 
14:  Set  $n = n + 1$ 
15: end while
16: return  $\mathbf{y}^n$ 

```

The update immediately after the backtracking and restarting gives us $\eta^{n+1} = 0$ and $\mathbf{w}^{n+1} = \mathbf{y}^{n+1} = \mathbf{y}^n$, which further implies that the immediate next step with (2.5) (resp. (2.25)) is a gradient flow update with time step τ^2 . This gives an estimate by [14, 18] in the form of (2.13) and (2.32) with steps $n + 1, n + 2$, and guarantees a monotone decreasing of potential energy $E = E_{pre}$ (resp. E_{bi}).

On the continuous level, i.e., referring to (2.9), such backtracking and restarting scheme could correspond to some discontinuous damping coefficients, which brings more challenges analytically. Additionally, we emphasize that this strategy does not apply to the scenario of $\eta^n = 1 - \beta\tau$ (heavy ball method) directly, as η^n remains constant in the flow. A potential adjustment may involve modifying β in the flow to enable a gradient flow step for reducing E . We defer the exploration of such a time-dependent β to future studies.

3.1.2. High order approximation of constraints. Inspired by [1] for gradient flows, we modify (2.5) corresponding to a BDF2 approximation of time derivative

$$\dot{\mathbf{y}}^n \approx \frac{3\mathbf{y}^n - 4\mathbf{y}^{n-1} + \mathbf{y}^{n-2}}{2\tau}.$$

This leads to a higher order approximation of constraints for the gradient flow algorithm in [1], and we expect to achieve similar improvements computationally for our accelerated flows. The new scheme is described in Algorithm 3.2. In essence, for any $n \geq 1$, at each step we compute increment in the tangent space with a specific extrapolation as in [1], namely $\delta\mathbf{y}^{n+1} \in \mathcal{F}(2\mathbf{y}^n - \mathbf{y}^{n-1})$, such that

$$(3.1) \quad \tau^{-2}(\delta\mathbf{y}^{n+1}, \mathbf{v})_{H^2} + \frac{2}{3}a_g(\delta\mathbf{y}^{n+1}, \mathbf{v}) = a_g(-\frac{4}{3}\mathbf{w}^n + \frac{1}{3}\mathbf{w}^{n-1}, \mathbf{v}) + \tau^{-2}(\mathbf{w}^n - \mathbf{y}^n, \mathbf{v})_{H^2}$$

The equation (3.1) is formulated for prestrained plates, and we can add the term $\ell[\mathbf{w}^n](\mathbf{v})$ to the right hand side and replace a_g by a for bilayer plates. We also need to modify the update of \mathbf{y}^{n+1} corresponding to the BDF2 scheme. The performance of Algorithm 3.2 is reported in Section 3.3, while an analysis like [1] remains open.

Algorithm 3.2 Accelerated flow with BDF2 strategy

- 1: Given a pseudo time-step $\tau > 0$, a tolerance tol and parameter $\alpha \geq 3$
 - 2: Choose $\mathbf{y}^0 \in \mathcal{A}$, set $\mathbf{w}^0 = \mathbf{y}^0$, $n = 0$, $k = 0$ and $\Delta E_{total} = \infty$
 - 3: Compute $\delta\mathbf{y}^1 \in \mathcal{F}(\mathbf{y}^0)$ by (2.5) (resp. (2.25))
 - 4: Update $\mathbf{y}^1 = \mathbf{y}^0 + \delta\mathbf{y}^1$, $\mathbf{w}^1 = \mathbf{y}^1$ and $n = n + 1$
 - 5: **while** $\tau^{-1}\Delta E_{total} > tol$ **do**
 - 6: **Solve** (3.1) for $\delta\mathbf{y}^{n+1} \in \mathcal{F}(2\mathbf{y}^n - \mathbf{y}^{n-1})$
 - 7: **Update** $\mathbf{y}^{n+1} = \frac{4}{3}\mathbf{y}^n - \frac{1}{3}\mathbf{y}^{n-1} + \frac{2}{3}\delta\mathbf{y}^{n+1}$
 - 8: **Set** $\Delta E_{total} = E_{total}[\mathbf{y}^{n+1}] - E_{total}[\mathbf{y}^n]$ and $\Delta E = E[\mathbf{y}^{n+1}] - E[\mathbf{y}^n]$
 - 9: **if** $\Delta E < 0$ **then**
 - 10: **Set** $k = k + 1$
 - 11: **else**
 - 12: **Backtrack** $\mathbf{y}^{n+1} = \mathbf{y}^n$
 - 13: **Restart** $k = 1$
 - 14: **end if**
 - 15: **Update** $\eta^{n+1} = \frac{k-1}{k-1+\alpha}$ and $\mathbf{w}^{n+1} = \mathbf{y}^{n+1} + \eta^{n+1}\delta\mathbf{y}^{n+1}$
 - 16: **Set** $n = n + 1$
 - 17: **end while**
 - 18: **return** \mathbf{y}^n
-

3.2. Spatial discretization: Morley FEM. In order to implement the algorithms that we have proposed, we also need to discretize the problems spatially to have full discretizations. In this work, we utilize Morley FEM for these problems and we provide a brief introduction in this subsection, while a detailed analysis is presented in our accompanying paper [21]. We emphasize that the semi-discrete schemes presented in Algorithms 2.1, 3.1, 3.2 should work when using any other suitable FEMs for spatial discretization, such as Kirchhoff FEM, IPDG, and LDG in previous studies on nonlinear plates models (1.1), (1.4), and (1.6).

We consider a shape-regular triangulation \mathcal{T}_h of $\Omega \subset \mathbb{R}^2$ fitted with the boundary $\partial\Omega$. We denote the set of vertices of the mesh \mathcal{T}_h as \mathcal{N}_h , and the set of edges as \mathcal{E}_h .

In particular $\mathcal{E}_h = \mathcal{E}_h^0 \cup \mathcal{E}_h^D$, where $\mathcal{E}_h^D := \{E \in \mathcal{E}_h : E \subset \Gamma^D\}$ is the set of Dirichlet boundary edges and $\mathcal{E}_h^0 := \mathcal{E}_h \setminus \mathcal{E}_h^D$. Similarly, we define $\mathcal{N}_h^D := \{z \in \mathcal{N}_h : z \subset \Gamma^D\}$. For any edge $E \in \mathcal{E}_h$, the midpoint of E is denoted as m_E . Moreover, $\boldsymbol{\nu} : \mathcal{E}_h \rightarrow \mathbb{S}^1$ denotes the unit normal vectors to each $E \in \mathcal{E}_h$, where its orientation is arbitrary but remains fixed upon selection. The Morley FEM was originally proposed in [29] with the *nonconforming* FE space:

$$\begin{aligned} \mathbb{V}_h = \{ & v_h \in L^2(\Omega) : v_h|_T \in \mathbb{P}_2(T), \forall T \in \mathcal{T}_h, v_h \text{ is continuous at } z, \forall z \in \mathcal{N}_h \\ & \nabla v_h \cdot \boldsymbol{\nu} \text{ is continuous at } m_E, \forall E \in \mathcal{E}_h \}. \end{aligned}$$

Moreover, we define the discrete space of vanishing boundary values as:

$$(3.2) \quad \mathbb{V}_h^D = \{v_h \in \mathbb{V}_h : \text{dofs of } v_h \text{ are vanishing on } E \in \mathcal{E}_h^D\}.$$

We next define the following useful quadrature rule for any $T \in \mathcal{T}_h$:

$$(3.3) \quad Q_T(\phi) := \frac{|T|}{3} \sum_{E \in \mathcal{E}_h^T} \phi(m_E),$$

where \mathcal{E}_h^T denotes the set of three sides of triangle and $|T|$ denotes the area of T . $Q_T(\phi)$ is an approximation of $\int_T \phi$. We define the discrete counterparts E_{pre}^h and E_{bi}^h to E_{pre} and E_{bi} for discrete deformations $\mathbf{y}_h \in [\mathbb{V}_h]^3$ as follows:

$$(3.4) \quad E_{pre}^h[\mathbf{y}_h] := \sum_{T \in \mathcal{T}_h} \frac{\mu}{12} \int_T \left| g^{-\frac{1}{2}} D^2 \mathbf{y}_h g^{-\frac{1}{2}} \right|^2 + \frac{\lambda}{2\mu + \lambda} \text{tr} \left(g^{-\frac{1}{2}} D^2 \mathbf{y}_h g^{-\frac{1}{2}} \right)^2,$$

and

$$(3.5) \quad E_{bi}^h[\mathbf{y}_h] := \sum_{T \in \mathcal{T}_h} \frac{1}{2} \int_T |D^2 \mathbf{y}_h|^2 - \sum_{i,j=1}^2 \sum_{T \in \mathcal{T}_h} Q_T(\partial_{ij} \mathbf{y}_h \cdot (\partial_1 \mathbf{y}_h \times \partial_2 \mathbf{y}_h) Z_{ij}).$$

In the practical implementation of accelerated flows in Algorithms 2.1, 3.1, and 3.2, considering the given $\mathbf{y}_h^n \in [\mathbb{V}_h]^3$, the linearized constraint at n -th step is

$$(3.6) \quad L_T(\mathbf{y}_h^n, \mathbf{v}_h) := Q_T(\nabla \mathbf{v}_h^T \nabla \mathbf{y}_h^n + (\nabla \mathbf{y}_h^n)^T \nabla \mathbf{v}_h) = 0.$$

Corresponding tangent space is $\mathcal{F}_h(\mathbf{y}_h^n) := \{\mathbf{v}_h \in [\mathbb{V}_h^D]^3 : L_T(\mathbf{y}_h^n, \mathbf{v}_h) = 0, \forall T \in \mathcal{T}_h\}$. These algorithms can be readily applied to the case with full discretization, upon replacing verbatim $E, \mathbf{y}, \mathbf{w}, \mathbf{v}, \mathcal{F}, H^2(\Omega), H_0^2(\Omega), |\cdot|_{H^2}$ respectively by $E^h, \mathbf{y}_h, \mathbf{w}_h, \mathbf{v}_h, \mathcal{F}_h, \mathbb{V}_h, \mathbb{V}_h^D, |\cdot|_h$, where $|\mathbf{v}_h|_h := (\sum_{T \in \mathcal{T}_h} \|D^2 \mathbf{v}_h\|_{L^2(T)}^2)^{1/2}$ defines a norm on \mathbb{V}_h^D .

3.3. Numerical tests. We first introduce the set-up of several benchmark numerical examples by which we illustrate the performance of our new method.

Example 1: Single layer plates with vertical load. We take a square domain $\Omega = (0, 4)^2$, and a vertical load $\mathbf{f} = (0, 0, 0.025)^T$. The plate is clamped on $\Gamma^D = \{0\} \times [0, 4] \cup [0, 4] \times \{0\}$, i.e. we prescribe the Dirichlet boundary condition with

$$(3.7) \quad \boldsymbol{\varphi}(x_1, x_2) = (x_1, x_2, 0)^T \quad \text{and} \quad \Phi = [I_2, \mathbf{0}]^T \quad (x_1, x_2) \in \Gamma^D.$$

The initial state is the flat plate $\mathbf{y}^0(x_1, x_2) = (x_1, x_2, 0)^T$. This is the simplest test example for nonlinear plates as in previous works [5, 17].

Example 2: Bilayer plates with isotropic curvature. We consider a rectangular plate $\Omega = (-5, 5) \times (-2, 2)$ clamped on the side $\Gamma^D = \{-5\} \times [-2, 2]$ with boundary condition (3.7). The spontaneous curvature is isotropic and takes form $Z = \gamma I_2$ with various values of γ . The exact solution to (1.1), i.e. deformation with minimal energy, is a cylinder of radius $1/\gamma$ and energy $20\gamma^2$ [35]. The initial state is the flat plate $\mathbf{y}^0(x_1, x_2) = (x_1, x_2, 0)^T$. In the rest of this section, we take $\gamma = 1$ in simulations unless specified (only in Section 3.3.4 we take $\gamma = 5$).

Example 3: Prestrained plates with various ratios of eigenvalues. We consider $\Omega = (-5, 5) \times (-2, 2)$ with the same boundary condition as in Example 2. We take metric g to be

$$(3.8) \quad g(x_1, x_2) = \begin{bmatrix} 1 + c^2(2(x_1 + 5)(x_1 - 2) + (x_1 + 5)^2) & 0 \\ 0 & 1 \end{bmatrix},$$

with the parameter c determining the ratios between two eigenvalues of $g(x_1, x_2)$ when (x_1, x_2) is away from Γ^D . The initial state is $\mathbf{y}^0(x_1, x_2) = (x_1, x_2, c(x_1 + 5)^2(x_1 - 2))$ satisfying $\mathbb{I}[\mathbf{y}^0] = g$. We set Lamé parameters to be $\mu = 12$ and $\lambda = 0$. In the rest part of this section, we take $c = 0.01$ or 0.1 , and the former corresponds to eigenvalues 3.56, 1 on $x_1 = 5$ while the latter gives eigenvalues 257, 1 on $x_1 = 5$. With these choices, we will study the performance of algorithms when eigenvalues are comparable or have a significant ratio.

3.3.1. Properties of accelerated flows. In this subsection, we present computational results that validates the properties of accelerated flows Algorithm 2.1, including total energy stability and control of constraint violation.

The behavior and results with varying τ of Algorithm 2.1 with the choice $\eta^n = \frac{n-1}{n-1+\alpha}$ (Nesterov's acceleration) are reported in Table 1 and Fig. 1 (left). The same outputs are reported in Table 2 for $\eta^n = 1 - \beta\tau$ (Heavy ball method). In our simulations, we measure discrete counterparts $D_{g,p}^h$ of $D_{g,p}$, which is defined by

$$(3.9) \quad D_{g,p}^h[\mathbf{y}_h] = \left(\sum_{T \in \mathcal{T}_h} \left| Q_T(\nabla \mathbf{y}_h^T \nabla \mathbf{y}_h - g) \right|^p \right)^{1/p}.$$

We have verified that $D_{g,p}^h \approx \mathcal{O}(\tau) \approx \mathcal{O}(N\tau^2)$ and $N \approx \mathcal{O}(\tau^{-1})$ for Example 1, 2 and 3, where $g = I_2$ for Example 1, 2 and g is given by (3.8) for Example 3. These results are consistent with our analysis for control of constraint violation as in Theorem 2.2, 2.4 and Remark 2.2. When comparing the two choices of η^n , we find out that the latter requires fewer iteration numbers N than the former, although it has larger violations $D_{g,p}^h$ and larger energy errors for Example 2, which has an exact energy 20.

Example 1				Example 2				Example 3			
τ	E_{si}^h	$D_{I_2,1}^h$	N	τ	E_{bi}^h	$D_{I_2,2}^h$	N	τ	E_{pre}^h	$D_{g,1}^h$	N
2^{-3}	-1.01E-2	1.1E-3	85	0.01	17.2365	0.0753	15935	0.05	0.2124	0.1743	923
2^{-4}	-1.01E-2	6.1E-4	174	0.005	17.3595	0.0374	32371	0.025	0.2112	0.0984	1848
2^{-5}	-1.01E-2	3.2E-4	348	0.0025	17.4194	0.0186	66966	0.0125	0.2105	0.0578	3698

TABLE 1

Computation of Example 1,2,3 using Algorithm 2.1 with $\eta^n = \frac{n-1}{n-1+\alpha}$, 512 elements and varying τ . Left: Example 1 with $\text{tol} = 10^{-6}$ and $\alpha = 3$. Middle: Example 2 with $\text{tol} = 10^{-4}$ and $\alpha = 6$. Right: Example 3 with $\text{tol} = 10^{-6}$, $\alpha = 3$ and $c = 0.01$.

Moreover, we confirm that the total energy E_{total} is monotonically decreasing in all the examples, while the potential energy $E = E_{bi}$ or E_{pre} often exhibits oscillations.

Example 1				Example 2				Example 3			
τ	E_{si}^h	$D_{I_2,1}^h$	N	τ	E_{bi}^h	$D_{I_2,2}^h$	N	τ	E_{pre}^h	$D_{g,1}^h$	N
2^{-3}	-1.01E-2	1.7E-3	56	0.01	17.0449	0.1211	9516	0.05	0.2122	0.2410	504
2^{-4}	-1.01E-2	9.4E-4	110	0.005	17.2628	0.0601	19190	0.025	0.2110	0.1376	978
2^{-5}	-1.01E-2	4.9E-4	218	0.0025	17.3704	0.0299	38543	0.0125	0.2104	0.0790	1925

TABLE 2

Computation of Example 1,2,3 using Algorithm 2.1 with $\eta^n = 1 - \beta\tau$, 512 elements and varying τ . Left: Example 1 with $\text{tol} = 10^{-6}$ and $\beta = 1$. Middle: Example 2 with $\text{tol} = 10^{-4}$ and $\beta = 0.2$. Right: Example 3 with $\text{tol} = 10^{-6}$, $\beta = 0.8$ and $c = 0.01$.

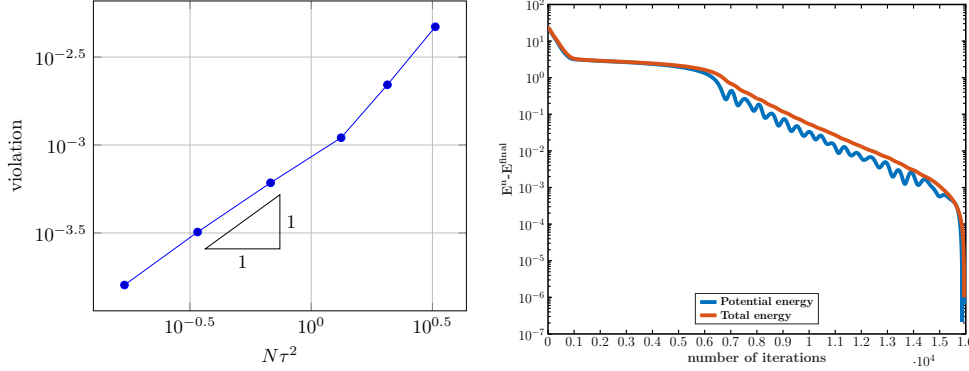


FIG. 1. Left: In the computation of Example 1 by Algorithm 2.1, violation of isometry constraint $D_{I_2,1}^h \approx \mathcal{O}(N\tau^2)$ asymptotically when τ is small. This matches our analysis. Right: Plot of E_{bi} and E_{total} for Example 2 computed with Algorithm 2.1.

This observation validates the total energy stability in Theorem 2.1, 2.4. Figure 1 (right) displays the change of E_{bi} and E_{total} over iterations in log scale for Example 2 computed by Algorithm 2.1.

Furthermore, we investigate the discrete kinetic energy $E_{ki}^h[\mathbf{y}_h^N] := \frac{1}{2\tau^2} |\delta \mathbf{y}_h^N|^2$ at the last step N of the accelerated flow in Algorithm 2.1. In Corollary 2.1, we have shown that for every fixed τ , the kinetic energy converges to 0 sequentially in the heavy ball dynamics, while for Nesterov's scheme, it converges to 0 sub-sequentially. However, in practice, N never goes to infinity and we stop the iterations when E_{total} stabilizes so that N is determined by τ with fixed tol as discussed in Remark 2.2 and shown in Table 1. Here, Table 3 indicates that $E_{ki}^h[\mathbf{y}_h^N]$ is decreasing as tol decreases and is usually 1 magnitude smaller than tol in practice. Despite the possible dependency of the constraint violation control constant ϵ on tol , as suggested in Remark 2.2, we observe in practice that $D_{I_2,1}^h$ stabilizes. Particularly when $\text{tol} \rightarrow 0$, $D_{I_2,1}^h$ appears to converge to a constant which shows the violation of the constraint (see Table 3). Additionally, the number of iterations N increases as tol decreases.

tol	1E-5	1E-6	1E-7	1E-8
$E_{ki}^h[\mathbf{y}_h^N]$	1.6E-6	7.4E-7	3.9E-8	7.1E-9
$D_{I_2,1}^h$	1.13E-3	1.14E-3	1.14E-3	1.14E-3
N	41	85	113	160

TABLE 3

Kinetic energy at last step, constraint violation and iteration number of Algorithm 2.1 versus values of tol . Computation of Example 1, with 512 elements, $\tau = 2^{-3}$ and $\alpha = 3$.

3.3.2. Role of α and β in accelerated flows. In this subsection, we investigate the influence of α and β on the performance of Algorithm 2.1 with the choices $\eta^n = \frac{n-1}{n+\alpha-1}$ and $\eta^n = 1 - \beta\tau$ respectively. We present how α affects total numbers of iterations and constraint violations for Example 1 in Fig. 2. We show the influence of β for Example 2 in Table 4.

In terms of the speed, $\alpha = 5$ is the best when $\tau = 2^{-2}$. When α is bigger than this value, the number of iterations increases with α . We note that the constraint violation decreases as α increases, and it stabilizes for large enough α . This is consistent with estimates in the proof of Theorem 2.2. In numerical simulations, we select the value of α that results in the fastest convergence, namely the fewest number of iterations. It is important to note that the rationale behind designing Algorithm 2.1 is to accelerate the flow, and higher values of α only lead to improvements of constants in constraint violation, not in its magnitudes. Moreover, it is also evident that the constraint violation increases as β decreases and the value of β influences the speed significantly.

We test α or β for various examples, it seems that the optimal-in-speed α or β mainly depends on data of problems and are influenced slightly by τ , but rather insensitive to meshsize h . This allows us to determine the optimal α or β using a relatively coarse mesh and then apply it to tests with further refinements. This helps us avoid spending a significant amount of computation time on selecting the optimal α or β .

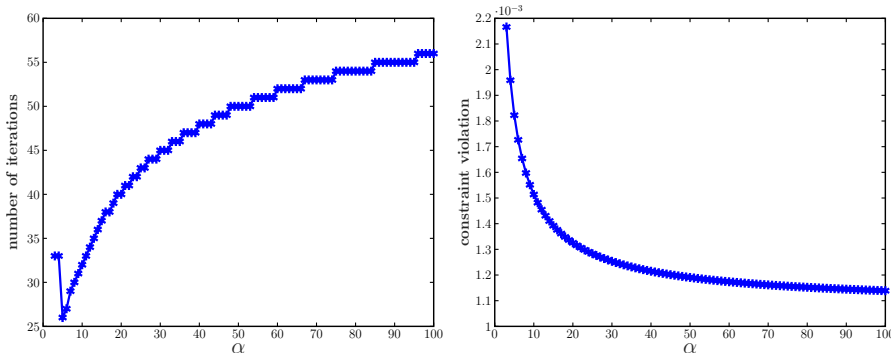


FIG. 2. Computation of Example 1 with various values of α , 512 elements, and $\tau = 2^{-2}$. Left: number of iterations N versus α . Right: constraint violation $D_{I2,1}^h$ versus α .

β	E_{bi}^h	$D_{I2,2}^h$	N
1	17.2583	0.0653	34829
0.5	17.1870	0.0833	18114
0.3	17.1168	0.1014	11246
0.2	17.0449	0.1211	9516
0.1	16.9075	0.1627	10477

TABLE 4

Numerical performance of Algorithm 2.1 with $\eta^n = 1 - \beta\tau$ for various β . Computation of Example 2 with 512 elements, $\tau = 0.01$, and $\text{tol} = 10^{-4}$.

3.3.3. Acceleration effect. In this section, we study the acceleration effect of accelerated flows in Algorithm 2.1 and its variation with backtracking/restarting

strategy in Algorithm 3.1, compared to gradient flow. In Fig. 3 (upper left) for Example 1, Algorithm 2.1 does not provide a speed advantage over gradient flow due to the simple structure of the single layer plate model, in which gradient flow already exhibits exponential decay. Similarly, Example 3 with $c = 0.01$, namely pretrained plates with two comparable eigenvalues of g , displays similar behavior. However, as shown in Fig. 3 (upper left), integrating the backtracking strategy into the accelerated flow enhances convergence speed, making it slightly more efficient than gradient flow. Furthermore, in Fig. 3 (upper right), we observe a considerable acceleration effect of Algorithm 2.1 for Example 2, the bilayer plates model, which exhibits additional non-convexity in its energy, causing gradient flows to encounter more challenges. In this example, the backtracking strategy further accelerates iterations, with Algorithm 2.1 being 2-3 times faster than gradient flows, while Algorithm 3.1 is 6-7 times faster. In Figure 3 (lower left) for Example 3 with $c = 0.1$ where the ratios of eigenvalues of g are significant, we observe that Algorithm 2.1 shows a more pronounced acceleration effect. In this scenario, the algorithm is 7-8 times faster than the gradient flow approach. Interestingly, when comparing Algorithm 2.1 with Algorithm 3.1 in this specific example, we find that the difference in performance is minimal, with E_{pre} exhibiting oscillations only near the end in the computation by Algorithm 2.1.

In all cases, we observe that the constraint violations are comparable for Algorithm 2.1, Algorithm 3.1 and gradient flow. Also, the potential energy is monotonically decreasing when the backtracking strategy is applied in Algorithm 3.1, as expected in the discussion of Section 3.1.1. Furthermore, we study the performance of Algorithm 3.1 for varying τ in Table 5. We still observe $D^h = \mathcal{O}(\tau)$ and $N = \mathcal{O}(\tau^{-1})$ in the case with backtracking. This reinforces the ability for backtracking to further accelerate the algorithms, as demonstrated by the comparison between Table 5 and Table 1.

τ	E_{si}^h	$D_{I_{2,1}}^h$	N
2^{-2}	-1.02E-2	2.1E-3	19
2^{-3}	-1.01E-2	1.1E-3	33
2^{-4}	-1.01E-2	5.7E-4	62

τ	E_{bi}^h	$D_{I_{2,2}}^h$	N
0.01	17.1742	0.0921	6008
0.005	17.3325	0.0454	12047
0.0025	17.4097	0.0225	24142

TABLE 5

Computation of Example 1,2 using Algorithm 3.1 (accelerated flow with backtracking) with 512 elements and varying τ . Left: Example 1 with $\text{tol} = 10^{-6}$ and $\alpha = 3$. Right: Example 2 with $\text{tol} = 10^{-4}$ and $\alpha = 3$.

3.3.4. Local and global minimizers. Computing global minimizers for these non-convex problems can be a challenging endeavor. When $Z = 5I_2$ in the bilayer plates model, i.e. in Example 2, with $\gamma = 5$, the exact solution is a cylinder with energy $E_{bi} = 500$, but it winds more times compared to the case when $Z = I_2$. However, previous gradient flow-based methods, such as [8, 16], have failed to produce a cylindrical shape at the end of the flow in this example, instead becoming stuck at a local minimum with a “dog’s ear” shape. In contrast, our accelerated flow Algorithm 2.1 has enabled us to reach a proper approximation of the cylindrical global minimizer. Snapshots of this evolution are displayed in Fig. 4. This experiment was conducted with a refinement of 8192 elements and $\tau = 0.005$.

3.3.5. Higher order approximation of constraints. In this section, we study the numerical performance of Algorithm 3.2 (accelerated flow with BDF2 scheme) with varying τ for Example 1 and 2, and the result is summarized in Table 6. We observe D^h converges even better than $\mathcal{O}(\tau^3)$, which outperforms the theory in [1] showing

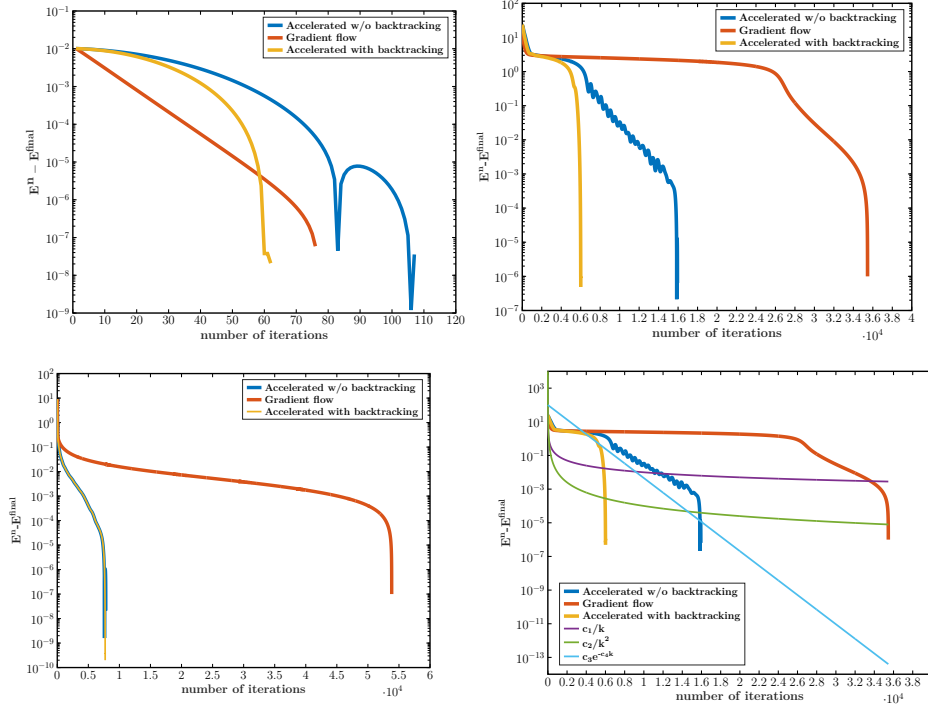


FIG. 3. Comparison between Algorithm 2.1 (accelerated gradient flows), Algorithm 3.1 (accelerated flows with backtracking) and gradient flows for Example 1,2,3. We take 512 elements in all the tests. We set $\tau = 2^{-4}, 0.01, 0.1$ for Example 1,2,3 respectively. Moreover, in Algorithm 2.1, $\alpha = 6$ for Example 1,2 and $\alpha = 3$ for Example 3. In Algorithm 3.1, $\alpha = 3$ for all the examples. We also set $c = 0.1$ in (3.8) for Example 3 in this test. The plot of E_{si} , E_{bi} and E_{pre} for Example 1,2,3 are shown as the upper left, upper right and lower left respectively. The lower right shows the convergence of energy E_{bi} for Example 2 versus ideal rate $\mathcal{O}(1/k)$ (for gradient flows), $\mathcal{O}(1/k^2)$ (for accelerated flows) and $\mathcal{O}(e^{-k})$.

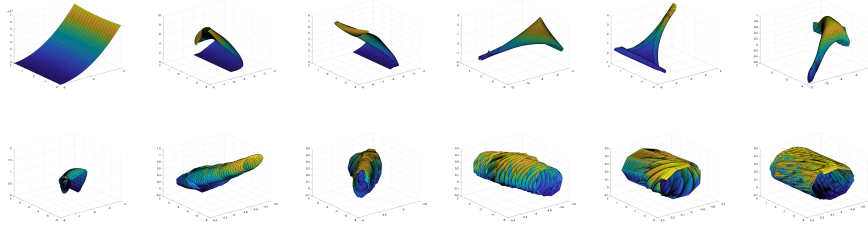


FIG. 4. Snapshots of evolution for bilayer plates with $Z = 5I_2$. From left to right, first row to second row: \mathbf{y}^n for $n = 1, 1k, 2k, 5k, 11k, 22k, 38k, 44k, 49k, 53k, 74k, 165k$. The “dog’s ear” shape appears in the process as a local minimizer, but the accelerated flow is able to drive the deformation to evolve into the cylindrical global minimizer in the end.

$D^h = \mathcal{O}(\tau^2)$ for the similar modifications to gradient flow method. The number of iterations N is almost $\mathcal{O}(\tau^{-1})$. It is important to note that the BDF2 scheme has a minimal influence on iteration numbers (convergence speed) comparing to results presented in Table 5.

As $\tau \rightarrow 0$ with fixed h and tol , we anticipate that $E^h[\mathbf{y}_h^{N(\tau)}] \rightarrow E^h[\mathbf{y}_h^*]$, where

$\mathbf{y}_h^{N(\tau)}$ is the solution obtained using our proposed algorithms with τ , and \mathbf{y}_h^* represents a discrete minimizer. Table 6 (right) illustrates that with Algorithm 3.2, the practical optimization error for Example 2 is on the order of 10^{-4} when τ decreases from 5×10^{-3} to 2.5×10^{-3} , outperforming previous gradient-flow methods in accuracy. For the bilayer example, the exact minimum energy is 20, and its difference from the stabilized value $E_{bi}^h \approx 17.4859$ is attributed to spatial discretization error with the current mesh. Furthermore, the optimization accuracy for the simpler single layer example (Example 1) is at the level of 10^{-7} when τ ranges from 2^{-4} to 2^{-6} ; see Table 6 (left).

In summary, Algorithm 3.2 (with backtracking enabled) has the best computational performance, while an analysis remains open.

τ	E_{si}^h	$D_{I_{2,1}}^h$	N	τ	E_{bi}^h	$D_{I_{2,2}}^h$	N
2^{-4}	-0.01010334	1.9E-6	63	0.01	17.4771	1.7E-5	7159
2^{-5}	-0.01010293	1.9E-7	121	0.005	17.4861	2.0E-6	12282
2^{-6}	-0.01010286	2.2E-8	238	0.0025	17.4859	2.4E-7	24372

TABLE 6

Computation of Example 1,2 using Algorithm 3.2 (accelerated flow with BDF2 and backtracking) with 512 elements and varying τ . Left: Example 1 with $\text{tol} = 10^{-6}$ and $\alpha = 3$. Right: Example 2 with $\text{tol} = 10^{-4}$ and $\alpha = 3$.

3.3.6. Convergence rate of accelerated flows. In unconstrained optimization of convex functions f , it is well-known that the accelerated flow of Nesterov type has a convergence rate $\mathcal{O}(1/k^2)$ (k is the iteration number) [30, 38]. It is challenging to extend such an analysis to these nonlinear plate models, where we need to solve (non-convex) energy functional minimization problems with non-convex constraints. Computationally, as shown in Fig. 3 (lower right), the ideal convergence rate $\mathcal{O}(1/k^2)$ for the accelerated flows is not satisfied at the beginning, and this is due to the non-convexity in these problems. As the iteration number k increases, the convergence rate $\mathcal{O}(1/k^2)$ is guaranteed, and it becomes exponential when approaching the minimizer. This indicates that these problems may become strongly convex in some small ‘neighborhood’ of a minimizer.

4. Conclusions. In this work, we have blended multiple strategies from diverse fields such as optimization and numerical PDEs to solve our non-convex problems. Our novel approaches resort to second-order dynamics based on Nesterov’s acceleration or the heavy ball method, a tangent space update strategy for effectively handling non-convex constraints, the backtracking technique, and the BDF2 approximation. By combining these techniques, we have developed a set of accelerated gradient flows that exhibit remarkable enhancements compared to existing methods when addressing non-convex constrained minimization problems associated with nonlinear plates. It is highly expected that our algorithms and analysis will also provide valuable insights into other non-convex variational problems with similar structures. While we have established energy stability and estimates on constraint violation, there are remaining open theoretical questions related to optimization. These include questions about the convergence to stationary points of the constrained optimization problems as the time-step vanishing, the convergence rates of proposed algorithms and high-order accuracy for constraint violation when integrating all the strategies mentioned, among others.

Acknowledgments. The work of G. Dong was supported by an NSFC grant 12001194. The work of H. G. was supported in part by the Andrew Sisson Fund, Dyason Fellowship, the Faculty Science Researcher Development Grant of the University of Melbourne.

REFERENCES

- [1] G. AKRIVIS, S. BARTELS, AND C. PALUS, *Quadratic constraint consistency in the projection-free approximation of harmonic maps and bending isometries*, arXiv preprint arXiv:2310.00381, (2023).
- [2] H. ATTOUCH, R. I. BOŦ, AND E. R. CSETNEK, *Fast optimization via inertial dynamics with closed-loop damping*, J. Eur. Math. Soc., 25 (2023), pp. 1985–2056.
- [3] H. ATTOUCH, Z. CHBANI, J. PEYPOUQUET, AND P. REDONT, *Fast convergence of inertial dynamics and algorithms with asymptotic vanishing viscosity*, Math. Program., 168 (2018), pp. 123–175.
- [4] H. ATTOUCH, X. GOUDOU, AND P. REDONT, *The heavy ball with friction method. I. The continuous dynamical system: global exploration of the local minima of a real-valued function by asymptotic analysis of a dissipative dynamical system*, Commun. Contemp. Math., 2 (2000), pp. 1–34.
- [5] S. BARTELS, *Approximation of large bending isometries with discrete kirchhoff triangles*, SIAM Journal on Numerical Analysis, 51 (2013), pp. 516–525.
- [6] S. BARTELS, *Projection-free approximation of geometrically constrained partial differential equations*, Mathematics of Computation, 85 (2016), pp. 1033–1049.
- [7] S. BARTELS, A. BONITO, A. H. MULIANA, AND R. H. NOCHETTO, *Modeling and simulation of thermally actuated bilayer plates*, Journal of Computational Physics, 354 (2018), pp. 512–528.
- [8] S. BARTELS, A. BONITO, AND R. H. NOCHETTO, *Bilayer plates: Model reduction, Γ -convergent finite element approximation, and discrete gradient flow*, Communications on Pure and Applied Mathematics, 70 (2017), pp. 547–589.
- [9] S. BARTELS AND C. PALUS, *Stable gradient flow discretizations for simulating bilayer plate bending with isometry and obstacle constraints*, IMA Journal of Numerical Analysis, 42 (2022), pp. 1903–1928.
- [10] K. BHATTACHARYA, M. LEWICKA, AND M. SCHÄFFNER, *Plates with incompatible prestrain*, Archive for Rational Mechanics and Analysis, 221 (2016), pp. 143–181.
- [11] R. BOŦ, G. DONG, P. ELBAU, AND O. SCHERZER, *Convergence rates of first- and higher-order dynamics for solving linear ill-posed problems*, Found. Comput. Math., 22 (2022), p. 1567–1629.
- [12] A. BONITO, D. GUIGNARD, AND A. MORVANT, *Finite element methods for the stretching and bending of thin structures with folding*, arXiv preprint arXiv:2311.04810, (2023).
- [13] A. BONITO, D. GUIGNARD, AND A. MORVANT, *Numerical approximations of thin structure deformations*, Comptes Rendus. Mécanique, 351 (2023), pp. 1–37.
- [14] A. BONITO, D. GUIGNARD, R. H. NOCHETTO, AND S. YANG, *LDG approximation of large deformations of prestrained plates*, Journal of Computational Physics, 448 (2022), p. 110719.
- [15] A. BONITO, D. GUIGNARD, R. H. NOCHETTO, AND S. YANG, *Numerical analysis of the LDG method for large deformations of prestrained plates*, IMA Journal of Numerical Analysis, 43 (2023), pp. 627–662.
- [16] A. BONITO, R. H. NOCHETTO, AND D. NTOGKAS, *Discontinuous galerkin approach to large bending deformation of a bilayer plate with isometry constraint*, arXiv preprint arXiv:2002.00114, (2020).
- [17] A. BONITO, R. H. NOCHETTO, AND D. NTOGKAS, *DG approach to large bending plate deformations with isometry constraint*, Mathematical Models and Methods in Applied Sciences, 31 (2021), pp. 133–175.
- [18] A. BONITO, R. H. NOCHETTO, AND S. YANG, *Γ -convergent ldg method for large bending deformations of bilayer plates*, arXiv preprint arXiv:2301.03151, (2023).
- [19] H. CHEN, G. DONG, W. LIU, AND Z. XIE, *Second-order flows for computing the ground states of rotating bose–einstein condensates*, J. Comput. Phys., 475 (2023), p. 111872.
- [20] E. E. CHUKWUMENKA AND S. W. WALKER, *Accelerated gradient descent methods for the uniaxially constrained landau-de gennes model*, Advances in Applied Mathematics and Mechanics, 14 (2021), pp. 1–32.
- [21] G. DONG, H. GUO, AND S. YANG, *Morley finite element discretization for large bending deformations of nonlinear plates*, in preparation.

- [22] G. DONG, M. HINTERMUELLER, AND Y. ZHANG, *A class of second-order geometric quasilinear hyperbolic PDEs and their application in imaging*, SIAM J. Imaging Sci., 14 (2021), pp. 645–688.
- [23] E. EFRATI, E. SHARON, AND R. KUPFERMAN, *Elastic theory of unconstrained non-euclidean plates*, Journal of the Mechanics and Physics of Solids, 57 (2009), pp. 762–775.
- [24] Y. FORTERRE, J. M. SKOTHEIM, J. DUMAIS, AND L. MAHADEVAN, *How the venus flytrap snaps*, Nature, 433 (2005), pp. 421–425.
- [25] A. GORIELY AND M. B. AMAR, *Differential growth and instability in elastic shells*, Physical review letters, 94 (2005), p. 198103.
- [26] X. LI, Y. LIAO, AND P. MING, *A pre-training deep learning method for simulating the large bending deformation of bilayer plates*, arXiv preprint arXiv:2308.04967, (2023).
- [27] X. LI AND P. MING, *Specht triangle approximation of large bending isometries*, Ann. Appl. Math, 10, pp. 1–28.
- [28] M. LOVE, P. ZINK, R. STROUD, D. BYE, S. RIZK, AND D. WHITE, *Demonstration of morphing technology through ground and wind tunnel tests*, in 48th AIAA/ASME/ASCE/AHS/ASC structures, structural dynamics, and materials conference, 2007, p. 1729.
- [29] L. S. D. MORLEY, *The triangular equilibrium element in the solution of plate bending problems*, The Aeronautical Quarterly, 19 (1968), pp. 149–169.
- [30] Y. NESTEROV, *A method of solving a convex programming problem with convergence rate $O(1/k^2)$* , Sov. Math. Dokl., 27 (1983), p. 372–376.
- [31] Y. NESTEROV, *Introductory Lectures on Convex Optimization: A Basic Course*, Appl. Optim., Vol. 87, Springer, New York, 2004.
- [32] R. H. NOCHETTO, M. RUGGERI, AND S. YANG, *Gamma-convergent projection-free finite element methods for nematic liquid crystals: The ericksen model*, SIAM Journal on Numerical Analysis, 60 (2022), pp. 856–887.
- [33] B. T. POLYAK, *Some methods of speeding up the convergence of iteration methods*, USSR Comput. Math. Math. Phys., 4 (1964), pp. 1–17.
- [34] M. RUMPF, S. SIMON, AND C. SMOCH, *Finite element approximation of large-scale isometric deformations of parametrized surfaces*, SIAM Journal on Numerical Analysis, 60 (2022), pp. 2945–2962.
- [35] B. SCHMIDT, *Minimal energy configurations of strained multi-layers*, Calculus of Variations and Partial Differential Equations, 30 (2007), pp. 477–497.
- [36] B. SCHMIDT, *Plate theory for stressed heterogeneous multilayers of finite bending energy*, Journal de mathématiques pures et appliquées, 88 (2007), pp. 107–122.
- [37] G. STOYCHEV, S. ZAKHARCHENKO, S. TURCAUD, J. W. DUNLOP, AND L. IONOV, *Shape-programmed folding of stimuli-responsive polymer bilayers*, ACS nano, 6 (2012), pp. 3925–3934.
- [38] W. SU, S. BOYD, AND E. J. CANDÈS, *A differential equation for modeling Nesterov’s accelerated gradient method: Theory and insights*, J. Mach. Learn. Res., 17 (2016), pp. 1–43.
- [39] M. WANG AND J. XU, *The Morley element for fourth order elliptic equations in any dimensions*, Numer. Math., 103 (2006), pp. 155–169.